# Laser-Responsive Shape Memory Device to Program the Stepwise Control of Intraocular Pressure in Glaucoma

*Kyubae Lee, Wungrak Choi, Si Yeong Kim, Eon-Bee Lee, Won Take Oh, Jeongeun Park, Chan Hee Lee, Jihei Sara Lee, Hyoung Won Bae, Dong-Su Jang, Kang Suk Lee, Se Won Yi, Mi-Lan Kang, Chan Yun Kim,\* and Hak-Joon Sung\**

There is an unmet need in the glaucoma clinic to control changes in the intraocular pressure (IOP), i.e., patient-specific hypotony and tissue fibrosis-mediated ocular hypertension, owing to the fixed tube diameter of the glaucoma drainage device. As a potential solution, the tube diameter can be adjusted, depending on the IOP, by shape memory polymer (SMP) and clinical laser systems, which can control the energy level, focus, and frequency by minimizing untargeted influences. To develop a translatable device, a laser-responsive SMP with two additional elements: i) a tube with an intimal gel coating to release 5-fluorouracil as an anti-fibrotic drug and ii) a safety lock ring to block late hypotony in special cases is employed. When the SMP tube is inserted into a silicone tube and wrapped externally by the ring, intimal gel degradation and argon laser-triggered diameter increase enable a three-step IOP control. Sustained drug release of the intimal gel suppresses tissue fibrosis, and the ring prevents late hypotony by externally squeezing the silicone tube. The advanced design and functions are validated using computational in vitro and rabbit glaucoma models by determining clinic-friendly argon laser parameters.

## 1. Introduction

The current design of glaucoma devices has limitations in ensuring patient-specific precision.[1–3] Although the intraocular pressure (IOP) of each patient undergoes hypotonic and ocular hypertensive changes over time depending on glaucoma stages, current devices with fixed diameters and fibrosis-inducing properties, often hamper clinician-specified IOP control, which is based on the situation and disease progress. Clinician-operated controls of IOP are urgently required when dealing with patient-specific glaucoma cases, by considering dynamic parameters including pressure and flow.[4,5] Uncontrolled IOP upon implantation of a glaucoma drainage device progressively worsens the prognosis, resulting in impaired vision, and consequently, blindness. Silicone has long been used in current glaucoma drainage devices owing to its durability, controllable properties, and ease of fabrication of devices.[6,7] Despite the advantages, the inability to handle dynamic body conditions, such as structural changes, hampers the clinician-operated control of IOP in patients with glaucoma. In addition, it has been reported that presently available implantable materials often result in bacterial growth with biofilm formation,[8] which is another challenge that needs to be addressed. Hence, cross-disciplinary implementation of the

K. Lee, S. Y. Kim, W. T. Oh, J. Park, C. H. Lee, K. S. Lee, S. W. Yi, M.-L. Kang, H.-J. Sung
Department of Medical Engineering
Yonsei University College of Medicine
50–1 Yonsei-ro, Seodaemun-gu, Seoul 03722, Republic of Korea
E-mail: hj72sung@yuhs.ac
W. Choi, J. S. Lee, H. W. Bae, C. Y. Kim
Department of Ophthalmology
Institute of Vision Research
Yonsei University College of Medicine
50–1 Yonsei-ro, Seodaemun-gu, Seoul 03722, Republic of Korea
E-mail: kcyeye@yuhs.ac

E.-B. Lee
Laboratory of Veterinary Pharmacokinetics and Pharmacodynamics
College of Veterinary Medicine
Kyungpook National University
Daegu 41566, Republic of Korea
D.-S. Jang
Office of Research Affairs
Yonsei University College of Medicine
50–1 Yonsei-ro, Seodaemun-gu, Seoul 03722, Republic of Korea
K. S. Lee, S. W. Yi, M.-L. Kang, H.-J. Sung
TMD LAB Co., Ltd
6th Floor, 31, Gwangnaru-ro 8-gil, Seongdong-gu, Seoul 04799, Republic of Korea

material function and device design are required to help clinicians control the functions of glaucoma drainage device to deal with unpredictable IOP changes in patients with glaucoma.[9–12] In particular, pin-point control of target lesions has emerged as a current paradigm in clinics, along with recent advances in laser systems, to minimize untargeted influences.[13,14] This paradigm is suggested to promote clinician-specified remote control of tube diameter by incorporating clinically safe laser systems such that IOP is stably managed according to individual patient requirements during the course of glaucoma.

Glaucoma occurs because of the overfilling of aqueous humor (intraocular fluid) and the consequent increase in IOP.[15,16] Hence, for the past decades, silicone devices have been implanted into glaucomatous eyes to drain the fluid and control the IOP over time.[17–19] Regardless of the device type, the fixed diameter of the drainage tube and silicone material has been considered as common factors that cause critical problems. The first issue starts within two weeks of device implantation because the fixed diameter of the silicone tube generates a relatively large pressure difference. The consequent over-drainage of the flow results in hypotony (IOP < 6 mmHg).[20–22] If this situation aggravates, choroidal detachment occurs resulting in blindness, which underscores the need for a smaller diameter tube to suppress the IOP drop during the early phase of device implantation. A month after implantation, the second issue arises as the IOP now elevates or fluctuates from a state of hypotony into ocular hypertension (IOP > 20 mmHg) or hypotony range, because the elevation speed and period are patient-specific.[23,24] Hence, patient-specific control to increase the tube diameter in a stepwise fashion is necessary. Third, this uncontrollable change in IOP is strongly associated with fibrotic tissue formation, primarily owing to the nature of the silicone material, suggesting the need for an anti-fibrotic function of tube implantation.[25–28] At last, several months after device implantation, some patients exhibit a sudden drop in the IOP that induces choroidal detachment and blindness upon severe progression, which indicates the need for a safety lock to suppress the abnormal IOP drop as needed.[29] Hence, these problems should be addressed by upgrading the device function and material properties to enable clinician-specified control of IOP.

As a breakthrough solution for the pin-point control of device function, a laser-responsive shape memory polymer (SMP) was used to program a three-step increase in tube diameter (D) with the release of 5-Fluorouracil (5-FU) as an anti-fibrotic drug. Numerous studies have shown that the use of 5-FU during glaucoma surgery is associated with significant anti-fibrosis benefits in terms of lowering intraocular pressure postoperatively.[30,31] Together, two SMP devices were designed to control the patient-specific fluctuation of IOP upon clinical decision. First, a SMP tube underwent inner lumen loading with a gel containing an anti-fibrotic drug and then insertion into the silicone drainage tube to enable stepwise increases of the inner diameter of the drainage tube. Second, a SMP ring was used to wrap the drainage tube externally as a safety lock. The inner diameter (ID = 305 μm) of the drainage tube became the small D (ID = 50 μm) post insertion of the SMP tube, thereby preventing early hypotony as occurred often by the initial massive drainage upon device implantation. The hydrolytic degradation of the inner lumen gel enabled the gradual release of the anti-fibrotic drug to the in-

traocular side. As a result, the small D of the SMP tube became the medium D (ID = 200 μm) which was then increased to the large D (ID = 250 μm) upon exposure to argon laser, thereby suppressing patient-specific ocular hypertension. Furthermore, the safety lock ring was used to prevent late hypotony by squeezing the silicone tube like an external wrap using SMP blended with polycaprolactone (PCL) (SMP+PCL). In SMP, the addition of GMA units into inter-PCL chains rather than the chain ends enabled crosslinking into inter-chains, thereby reducing the crystallinity, hardness, and $T_m$ together. In contrast, blending of PCL with SMP increased the polymer crystallinity and hardness so that the squeezing force of safety lock ring could be increased, and the $T_m$ elevation prevented the co-incident operation of ring with the SMP tube because more E was required. In this way, the two SMP devices can help ophthalmologists to control the IOP of each glaucoma patient by considering progressive changes in the prognostic status of drainage device implantation.

## 2. Results

### 2.1. Clinical Justification for Programming SMP Tube Functions

Glaucoma occurs owing to the blockage of ocular fluid drainage and the consequent increase in IOP with optic nerve damage (**Figure 1**a). The implantation of the drainage device into the glaucomatous eye induces the outflow of intraocular fluid through the silicone tube, thereby reducing the IOP (Figure S1a, Supporting Information). The 12-month examination of patients with glaucoma ($n = 127$) after implantation of silicone tube devices justified the need for stepwise IOP control (Figure 1b) as follows: i) the fixed diameter of the drainage tube-induced hypotony owing to the over-drainage of intraocular fluid by generating excess negative pressure. ii) The IOP rapidly increased to the normal range within two weeks with unstable IOP fluctuations, resulting in an IOP in the ocular hypertension range until three months. iii) Despite the IOP remaining predominantly in the normal range afterward, in some patients, it deviated to the pathological ocular hypertension range until the twelfth month. Early hypotony induced anterior chamber shrinkage compared with normal healthy eyes (Figure S1b, Supporting Information), followed by choroidal detachment and blindness in severe cases (Figure 1c).

The material properties of the silicone device are such that they often caused tissue fibrosis associated with late ocular hypertension (Figure 1d). Glaucoma progression induced a gradual loss of vision, and the visual area of the eye decreased to 41% in glaucomatous eyes compared to 100% seen in normal eyes.

Five months postimplantation of the drainage device, the vision loss worsened (residual visual area: ≈33%), owing to ocular hypertension, which occurred primarily because of fibrotic tissue formation (Figure S1c, Supporting Information). Laser-responsive SMP tube and safety lock rings are proposed to address these issues, as the pin-point delivery of light energy increases the tube diameter and decreases the ring diameter by considering the IOP variation of each patient with minimization of untargeted influences (Figure 1e-top). The separate operation of tube and ring was enabled by the laser-based pin-point control, achieved by placing the two devices apart from each other. Moreover, the SMP tube was implanted into the eye, whereas the
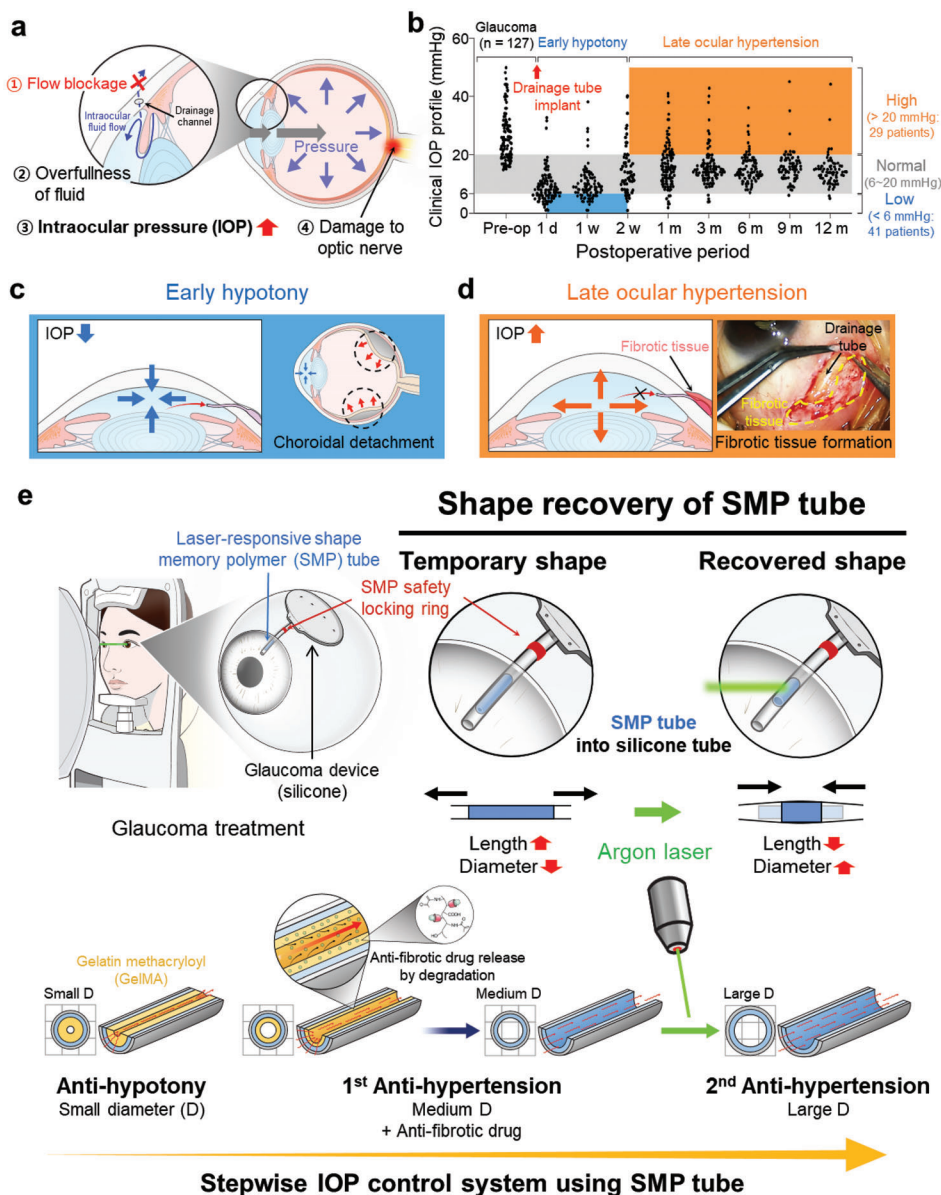
**Figure 1.** Glaucoma clinic-driven justification for using an SMP tube for the stepwise control of IOP. a) Glaucoma occurs when the ocular fluid drainage is blocked, resulting in an imbalance between production and drainage of fluid in the anterior chamber of eye, increased IOP, and optic nerve damage. b) The data from a 12-month examination of glaucoma patients ($n = 127$) justifies the clinical need for the stepwise control of IOP using an SMP tube: i) When the drainage device was implanted, the fixed diameter of tube lowered the high IOP to the hypotony range by over-draining intraocular fluid. ii) The IOP remained in the hypotony range for one week and then rapidly increased to the normal range within the next week, resulting in unstable IOP fluctuations in several patients to the ocular hypertension range until three months. iii) Despite remaining dominantly in the normal range afterward, in some patients, it deviated to the pathological ocular hypertension range until 12 months. c) The early hypotony induced anterior chamber shrinkage and choroidal detachment followed by blindness in severe cases. d) The properties of the silicone device often caused tissue fibrosis (dashed yellow line) during interaction with body fluid wastes, causing late ocular hypertension by incremental drainage blockage and tissue fibrosis. e) The laser-responsive shape memory tube was proposed to address the issues as the pin-point delivery of light energy promotes the fine control of diameter increase (shape recovery) by minimizing unexpected influences on neighboring tissues. The three steps of IOP control proceed from i) the small D by GelMA coating onto the intima to release anti-fibrotic drug, to ii) the medium D after GelMA degradation with drug release, and finally, to iii) the large D after diameter increase (shape recovery) upon pin-point exposure to the argon laser. SMP, shape memory polymer.

safety lock ring wrapped the silicone tube externally outside the eye, such that the ring position could be secured to avoid an overlap of laser exposure with the SMP tube. This setting was determined to minimize the influence of laser-based tube operation on the ring, thereby resulting in the operation of the two devices separately even though the same SMP material and argon laser system were used.

The SMP material was synthesized by ring-opening polymerization of $\epsilon$-caprolactone (CL) and glycidyl methacrylate (GMA) monomers (Figure S2a, Supporting Information). The successful

**ADVANCED
SCIENCE NEWS**

www.advancedsciencenews.com

**ADVANCED
FUNCTIONAL
MATERIALS**

www.afm-journal.de

synthesis was verified by analyzing the composition and molecular weight of the SMP material using proton nuclear magnetic resonance ($^1$H-NMR) (Figure S2b, Supporting Information) and gel permeation chromatography (GPC) (Figure S2c, Supporting Information), respectively. The GPC results exhibited the values of yield and polymerization degree to be 78% and 82%, respectively. The SMP material exhibited only 1.5% degradation in 1 year (Figure S2d, Supporting Information), based upon the accelerated aging test following the American Society of Testing and Materials (ASTM) international standard 1980, with preservation of the SMP function (97% shape fixity and 95% shape recovery) indicating a long-term stability. The recent approval of the use of the same SMP material as a nasolacrimal duct stent by the Korean Ministry of Food and Drug Safety supported the safety and durability of the SMP material. Gelatin was conjugated with methacrylic anhydride (GelMA) followed by conjugation with a complex of $\beta$-cyclodextrin ($\beta$-CD) and chloroacetic acid to produce GelMA-$\beta$-CD (Figure S3a, Supporting Information), as confirmed by $^1$H-NMR (Figure S3b–d, Supporting Information) and Fourier transform infrared (FTIR) spectroscopy (Figure S3e,f, Supporting Information). The carboxylic acid group was introduced into $\beta$-CD to react with the amino functional groups of GelMA molecule. Among several chemical modifications to introduce the carboxylic moiety, we chose chloroacetic acid to react with the hydroxyl groups on the $\beta$-CD, resulting in the formation of a carboxylic acid group[32,33] because this method is simple and generally accepted to obtain the desired yield.

Consequently, the three steps of IOP control proceed from: i) the small diameter (D) after GelMA-$\beta$-CD coating onto the intima to release the anti-fibrotic drug, ii) medium D after GelMA-$\beta$-CD degradation with drug release, and iii) large D after diameter increase (shape recovery) upon argon laser shots (Figure 1e-bottom).

## 2.2. Three-Step IOP Control and Drug Release by SMP Tube

Computational fluid dynamics (CFD) modeling was used to simulate the diameter (D), pressure, and velocity profiles and determine the length of the SMP tube for shape programming. The profiles were modeled after inserting the SMP tube into the silicone tube (length = 10 mm; inner D = 305 μm) of the glaucoma drainage device (Figure S4a, Supporting Information). When length of the SMP was set to 30 mm for insertion into the silicone tube, the postrecovery length was 15 mm. Consequently, D was changed from 50 μm (small D) to 200 μm (medium D) before and after GelMA-$\beta$-CD degradation, respectively, followed by a further increase to 250 μm (large D) upon shape recovery using argon laser shots. Accordingly, the CFD velocity increased markedly upon the insertion of the SMP tube and decreased to a level similar to that of the silicone tube only following the increased D, indicating stepwise control of the drainage flow rate and IOP. The findings of CFD modeling indicated a possibility to enable the three-step control of IOP with the SMP because the pressure difference ($\Delta P$) increased from 0.015 (silicone D w/o SMP tube) to 6.352 mmHg (small D), which indicates a resistance to the drop in IOP, thereby preventing hypotony (**Figure 2**a). Then, $\Delta P$ decreased to 0.036 (medium D) and 0.018 mmHg (large D), thereby controlling ocular hypertension shifts in a user-specified manner by stepwise increases in tube diameter.

Shape programming of the SMP tube was conducted following the shape memory cycle (Figure S4b, Supporting Information), as visualized by scanning electron microscopy (SEM), to bring about stepwise increases in tube diameter from 50 μm (small D) to 200 μm (medium D) before and after the degradation of drug-loaded GelMA-$\beta$-CD, respectively, followed by a further increase to 250 μm (large D) upon shape recovery (Figure 2b). The progressive changes in D were validated in vivo for 21 days postimplantation of SMP tube into the eyes, as GelMA-$\beta$-CD degraded until day 14 (before laser); moreover, argon laser shots at day 14 increased the D as programmed, which was confirmed at day 21 (after laser) (Figure S4c, Supporting Information). The increases in tube inner diameter from Small D to Medium D were a result of gel degradation and did not affect a change in outer diameter. During shape programming, the SMP tube was pulled on both sides and fixed to reduce not only inner diameter but also outer diameter. The next diameter expansion from Medium D to Large D was induced upon shape recovery, using argon laser shots (Figure S4d, Supporting Information). Thus, argon laser-triggered shape recovery resulted in increase of both inner and outer diameter. The hyper-elastic property of the silicone tube supported the stepwise expansion of SMP tube diameter.

A custom-built system was operated under a constant flow rate (25 μL min$^{-1}$) using a silicone drainage tube, with and without the SMP tube (Figure 2c). The resistance to pressure drops increased markedly over time, from prior to the SMP tube insertion to after insertion of the SMP tube at a diameter of small D, followed by a stepwise decrease in resistance at a diameter of medium D and further to the large D, after 700 s (Figure 2d). The silicone tube (without the SMP tube) resulted in the down-to-up fluctuation of IOP during 300$^{th}$–600th second when a drop of intraocular fluid was generated at the end of each test tube upon continuous slow flow. The silicone tube was affected specifically because of its hyper-elastic property. Hence, the lumen of the silicone tube appeared to shrink and re-open because the drop of intraocular fluid left a void volume inside the tube, which was then refilled by the fluid flow. $\beta$-CD was conjugated to GelMA to increase the loading capacity of 5-FU (Figure 2e), as confirmed by $^1$H-NMR (Figure 2f), resulting in an increase in the loading capacity by almost 10 times compared to GelMA only (Figure 2g). As the concentration of GelMA-$\beta$-CD increased (5, 7, and 10% w/v), the in vitro degradation slowed down for 14 days at 37 °C (Figure 2h), suggesting an effective means to control the speed of IOP drop and drug release. As an analytical point of 5-FU drug release kinetics, the $\beta$-CD conjugation to GelMA (5% w/v) resulted in the sustained release of 5-FU over 14 days due to the formation of GelMA-$\beta$-CD/5-FU complex in contrast to the burst release from GelMA only as a control (Figure 2i), indicating different release mechanisms between the two groups. The sustained release by GelMA-$\beta$-CD/5-FU complex was likely driven by hydrolytic degradation of the gel post stable entrapment of the drug because the 5-FU release was accelerated as the GelMA-$\beta$-CD weight decreased. On the other hand, the burst release of GelMA/5-FU appeared to be due to the simple mixing between the gel and drug as 5-FU was released rapidly in the initial phase,
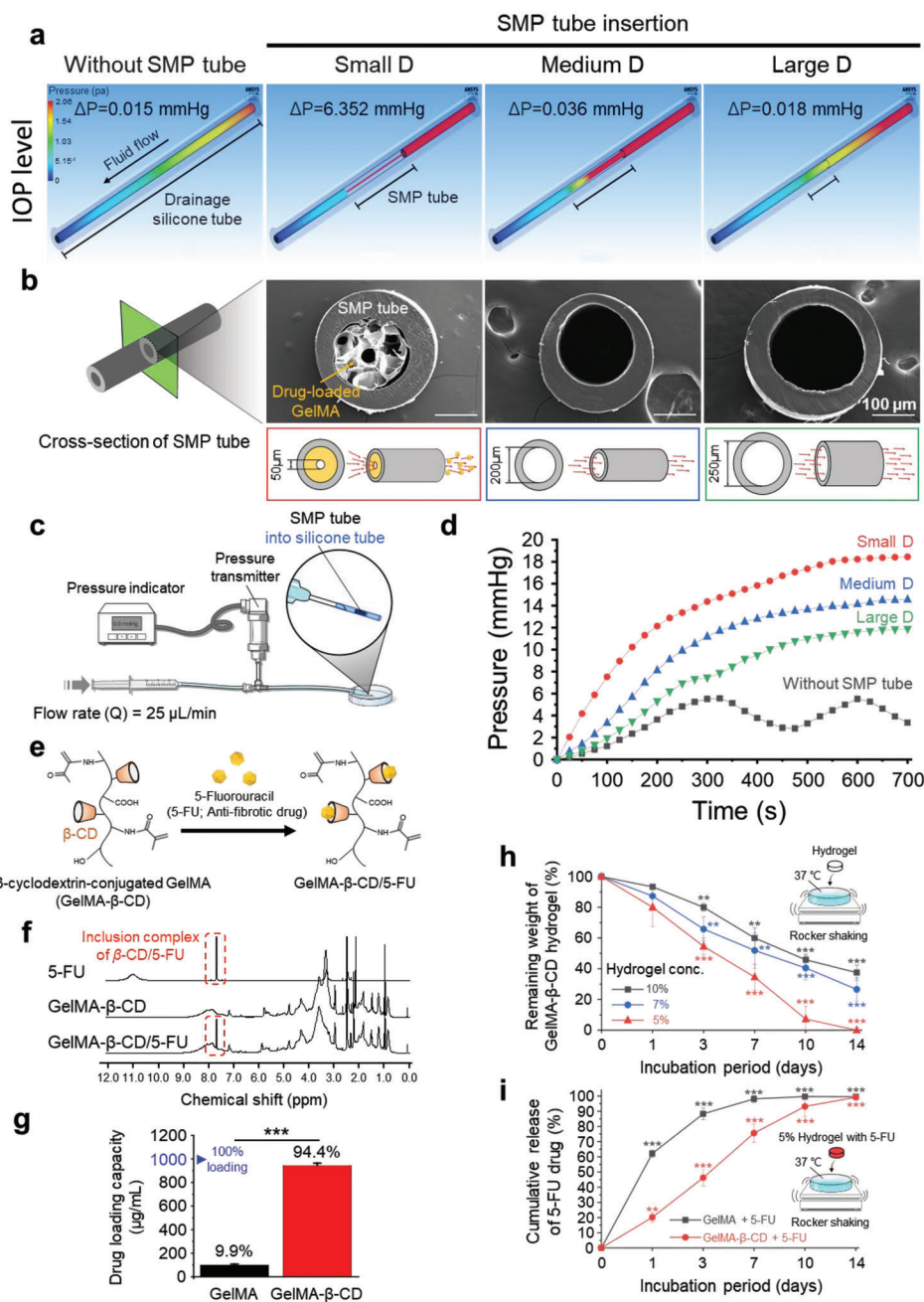
**ADVANCED
SCIENCE NEWS**

www.advancedsciencenews.com

**ADVANCED
FUNCTIONAL
MATERIALS**

www.afm-journal.de

**Figure 2.** Verification of three-step IOP control and anti-fibrotic drug release by the SMP tube using computational and analytical experiments. a) CFD simulations assisted the modeling of three-step IOP control by SMP because $\Delta P$ increased from 0.015 (silicone D w/o SMP tube) to 6.352 mmHg (small D), which indicates a resistance to the drop in IOP, thereby preventing hypotony. Then, $\Delta P$ decreased to 0.036 (medium D) and 0.018 mmHg (large D) to control ocular hypertension shifts in a user-specified manner via stepwise increases of the tube diameter. b) SEM visualized the stepwise increases of tube diameter from 50 µm (small D) to 200 µm (medium D) before and after the degradation of drug-loaded GelMA, respectively, followed by a further increase to 250 µm (large D) upon shape recovery. c) A pressure measurement system under a constant flow rate (25 µL min⁻¹) was custom-built using a silicone drainage tube with and without the insertion of the SMP tube. d) This system confirmed the SMP tube function as the pressure drop resistance increased significantly from the value without the SMP tube to that for small D over time, followed by stepwise decreases to medium D and further to large D at the end of 700 s (s). e) $\beta$-cyclodextrin (CD) was conjugated to GelMA (GelMA-$\beta$-CD) to increase the loading capacity of the anti-fibrotic drug (5-FU). f) The successful production of GelMA-$\beta$-CD with 5-FU loading was confirmed by proton nuclear magnetic resonance ($^1$H-NMR) spectroscopy. g) $\beta$-CD conjugation to GelMA increased the loading capacity of 5-FU by almost 10 times compared to GelMA only. The percentage value indicates the amount of drug that was loaded to each test group when loading of 1000 µg 5-FU was considered as full loading or 100%. h) As the concentration of GelMA-$\beta$-CD increased (5, 7, and 10% w/v), the in vitro degradation slowed down for 14 days at 37 °C, suggesting its effectiveness in controlling the speeds of IOP drop and drug release. i) $\beta$-CD conjugation to GelMA (5% w/v) enabled the sustained release of 5-FU drug for 14 days in vitro in contrast to the burst release by GelMA only. Data = mean ± standard deviation (*n* = 3). ** *p* < 0.01; *** *p* < 0.001 between lined groups or versus day 0 from one-way ANOVA with Tukey's post hoc test.

**ADVANCED
SCIENCE NEWS**

www.advancedsciencenews.com

**ADVANCED
FUNCTIONAL
MATERIALS**

www.afm-journal.de

indicating that the gel did not effectively entrap the drug. Furthermore, a pharmacokinetic (PK) analysis was performed to provide comprehensive insight into the drug release. Because tissue fibrosis has been an issue of current drainage devices, this issue was approached to address through the sustained release of 5-FU drug which was evidenced by the longer half-life ($T_{1/2}$) and mean residence time (MRT) with the increased area under the concentration-time curve (AUC) (Figure S5, Supporting Information). Therefore, GelMA-$\beta$-CD/5-FU complex was used as a strategy to enable sustained drug release in the follow-up experiments.

### 2.3. Clinic-Friendly Setting of SMP Tube Operation

During shape programming, the 1.5 mm long tube (recovery shape) was elongated at 55 °C and fixed in cold water at 4 °C so that the diameter decreased, followed by cutting to a 3 mm long tube (insertion shape) based on Poisson's ratio ($v = 0.2$) of the SMP (**Figure 3**a). The SMP tube was painted black to promote laser absorption, and argon laser shots in the clinical room induced the expansion of the tube diameter by decreasing its length (Figure 3b). Warm water can also be used, although it spreads into the neighboring areas.[34] However, calculations confirmed the superior energy efficiency ($\approx$66 times) of the argon laser (energy density: $\approx$4286 J cm$^{-3}$) through pin-point shot delivery when compared to the water heat energy ($Q_{water}$: $\approx$65 J cm$^{-3}$ at 50 °C) (Figure 3c; Figure S6, Supporting Information), indicating another advantage in minimizing unexpected influences on neighboring tissues.[35]

The efficiency of the argon laser energy ($E$) was tuned in the following two steps to determine the maximum $E$ of a single shot within the clinical safety range (Figure 3d,e). This minimized the number of laser shots so that the pin-point laser focusing remained undisturbed. First, as the low-$E$ shot resulted in nonlinear shape recovery (e.g., bending), the minimum $E$ of a single shot for linear recovery within the clinically safe range (max. 70 mJ) was determined to be 40 mJ (Figure 3d; Video S1, Supporting Information). Next, the critical $E$ of a single shot for shape recovery was determined as 60 mJ to minimize the number of laser shots because the shape recovery ratio did not improve significantly between 60–70 mJ (safety limit) (Figure 3e). The SMP tube was inserted into a silicone tube, which was implanted into an eye where aqueous humor was filled, and the argon laser parameters were set following the previous clinical experiences. Therefore, any thermal injury to neighboring eye tissues did not appear during the laser exposure time to activate the diameter increase by shape recovery.

### 2.4. Rescue of Glaucomatous Rabbit Eyes by SMP Tube

An SMP tube was inserted into a silicone tube with external wrapping by the SMP+PCL ring (SMP: black), which was implanted into glaucomatous eyes in a rabbit model (**Figure 4**a). The SMP device suppressed the near hypotony of the silicone tube only (w/o SMP tube) for 10 days by changing from small D to medium D owing to GelMA-$\beta$-CD degradation with the release of the anti-fibrotic drug (Figure 4b). Then, the change from medium D to

large D of the SMP tube by argon laser shots lowered the ocular hypertension of the silicone tube only (w/o SMP tube) to the normal range until 42 days (Video S2, Supporting Information). The beneficial effect of change in inner tube diameter from medium D to large D by argon laser shots (+ laser w/SMP) suppressed the incremental change in IOP until day 21. Also, the incremental levels of the SMP tube group with no laser shot (-Laser w/SMP tube) remained lower than those without the SMP tube (silicone tube only) due to anti-fibrotic functions (Figure 4c). Herein, the measurements were performed on day 21 and not day 42 (Figure 4b). This was because the effect of diameter expansion started to show an attenuation from days 15 to 16 (i.e., 1–2 days after laser exposure), as the + laser group moved to the incremental IOP stage until day 21.

As the eye temperature was 34.3 °C (Figure S6, Supporting information) in alignment with a previous study,[36] the groups with saline treatment at 25 °C and 50 °C to induce shape recovery were compared upon intraocular versus extraocular implantation of the SMP tube (Figure S7, Supporting Information). Here, these two temperatures represent the lowest (room temperature) and highest (protein denature point) sets, respectively, considering 34.3 °C as standard eye temperature. Even the saline at 50 °C could not induce shape recovery in the intraocular position, but succeeded in the extraocular position, as demonstrated by the shortened tube length (Video S3, Supporting Information). It indicates the limitation of water heat in inducing shape recovery owing to insufficient energy transfer to the intraocular position, which was further supported by no shape change by the saline treatment at 50 °C. The result also supports the superior energy efficiency ($\approx$66 times) of the argon laser when compared to water at 50 °C (Figure 3c).

The release of the anti-fibrotic drug (5-FU) from GelMA-$\beta$-CD in the SMP tube (small D) helped to maintain normal histological features by suppressing fibrotic tissue formation. Moreover, $\beta$-CD conjugation to GelMA enabled the sustained release of anti-fibrosis drug, avoiding the sudden drops of IOP levels. Although $\beta$-cyclodextrin ($\beta$-CD) is known to improve drug loading and to enable sustained release, the drug activity could still be attenuated. Recent studies have reported that the $\beta$-CD/anti-fibrosis drug complex also has the ability to exert the anti-fibrosis function despite the reduced drug activity.[37–39] Indeed, in the present setting, the $\beta$-CD conjugation did not significantly affect the anti-fibrotic activity of 5-FU, as evidenced by the results of hematoxylin and eosin (H&E) and Masson's trichrome staining (Figure 4d). The in vitro release upon incubation in PBS with collagenase indicates the combined mechanisms of hydrolysis and enzymatic degradation (Figure 2h,i). However, the in vivo release confirms hydrolytic degradation as a main mechanism in alignment with a previous study[40,41] because collagenases might not exist sufficiently in the intraocular fluid.[42]

Several biocompatible properties of SMP materials have been reported, even though these properties have not been fully investigated in glaucoma drainage devices: i) the SMP material was found to be safe in terms of excellent performance, with no evidence of toxic and immune-rejection upon implantation in rabbits, pigs, dogs, and rodents as reported previously.[34,43–45] ii) The Korean Ministry of Food and Drug safety approved the use of SMP material for an eye device (i.e., nasolacrimal duct stent),
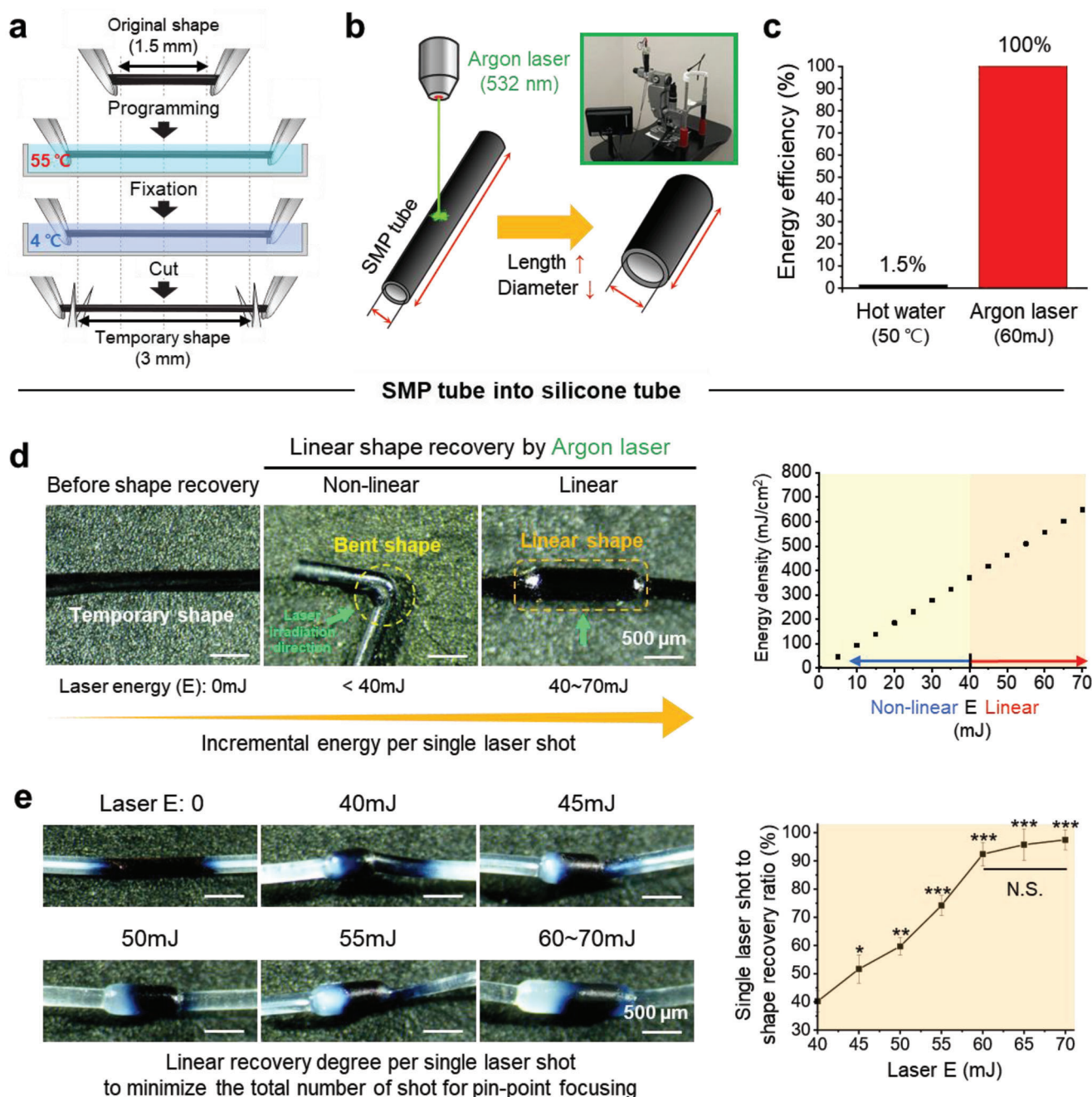
**Figure 3.** Shape programming of the SMP tube by tuning the clinic-friendly laser parameter. a) During the shape programming process, the 1.5 mm long tube (recovery shape) was elongated in hot water (55 °C) and fixed in cold water (4 °C) to reduce the diameter, followed by cutting to a 3 mm long tube (temporary shape) based on the Poisson's ratio ($\nu = 0.2$) of the SMP. The SMP tube was painted black to promote laser absorption. b) After administering argon laser shots in the clinical room, the shape recovery was tested to validate the expansion of tube diameter by decreasing the length. c) The pin-point shot delivery of laser energy (E) was more efficient ($\approx 66$ times) compared to hot water (50 °C), indicating its advantage in minimizing untargeted influences. d-e) Two-step characterization of laser E efficiency was performed to determine the maximum E of a single shot within the clinical safety range and minimize the shot number to maintain the pin-point laser focusing. d, First, because the low E shot resulted in nonlinear shape recovery (e.g., bending), the minimum E of a single shot for linear recovery within the clinical safety range (max. 70 mJ) was determined as 40 mJ. e, Next, the critical E of a single shot for shape recovery was determined as 60 mJ to minimize the number of laser shots, because the shape recovery ratio between 60 and 70 mJ (safety limit) was not significantly improved. Data = mean ± standard deviation ($n = 3$). * $p < 0.05$; ** $p < 0.01$; *** $p < 0.001$ versus 40 mJ from one-way ANOVA with Tukey's post hoc test (N.S.: not significant).
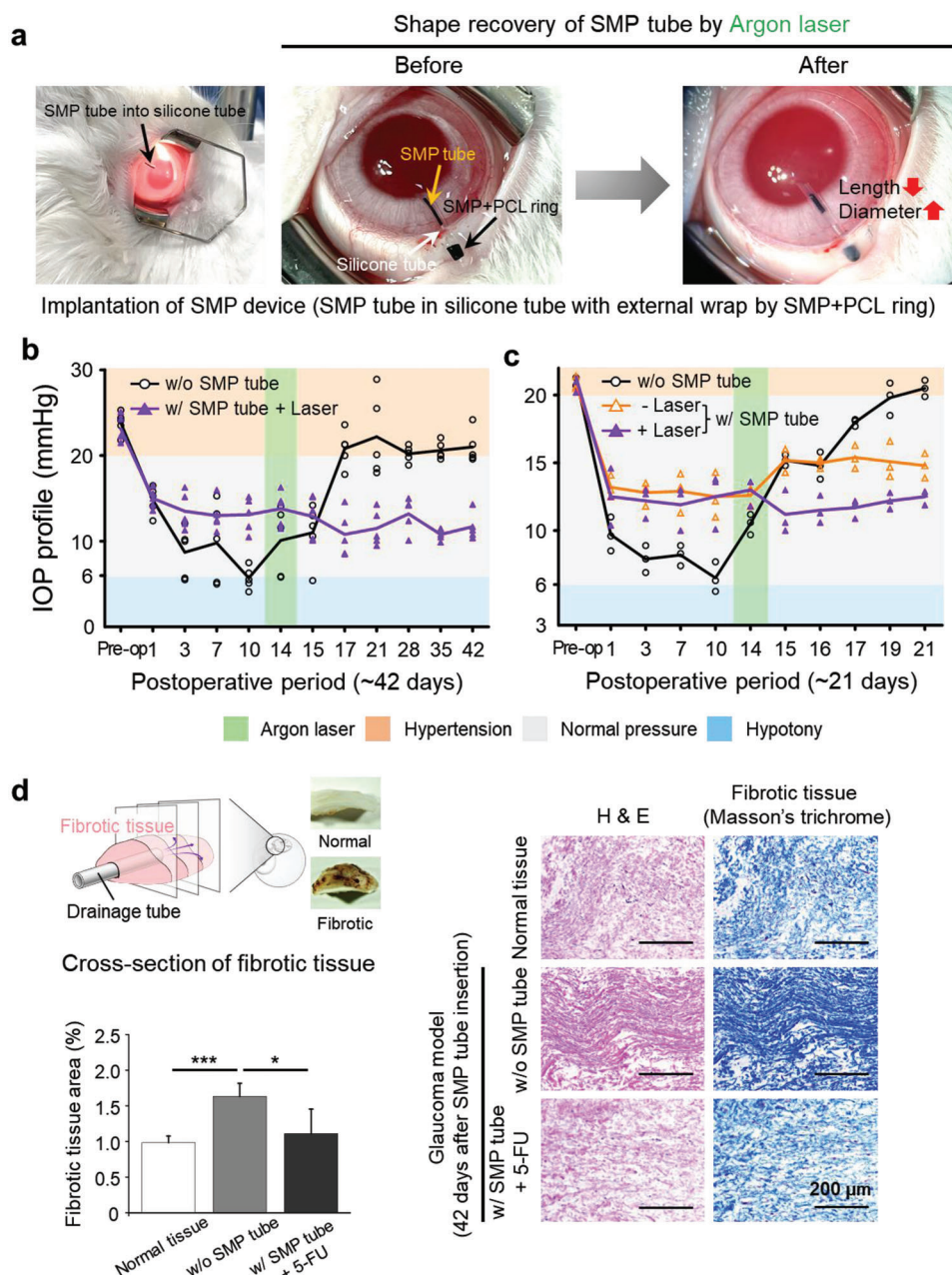
**Figure 4.** Treatment of glaucomatous rabbit eyes using the SMP tube with stepwise diameter recovery and anti-fibrotic drug release. a) The SMP device was produced by inserting the SMP tube into a silicone tube (part of the glaucoma device) with external wrapping by an SMP+PCL ring as a safety lock to prevent late hypotony (See Figure 5 for details). The SMP device was implanted into glaucomatous eyes in a rabbit model and tested to validate the diameter increase by decreasing the length using argon laser shots. b) In the rabbit glaucoma model, the implantation of the SMP device suppressed the near hypotony (w/o SMP tube) for 10 days by changing from small D to medium D SMP tube, owing to the complete degradation of GelMA-$\beta$-CD with complete release of the anti-fibrotic drug. Then, the change from medium D to large D SMP tube by argon laser shots lowered ocular hypertension (w/o SMP tube) to the normal range until 42 days ($n = 5$ rabbits). c) The beneficial effect of changing the inner tube diameter from medium D to large D by argon laser shots (+ laser w/SMP) suppressed the incremental change in IOP in the rabbit glaucoma model until day 21. Furthermore, the incremental level in the SMP tube group without laser shot (-Laser w/SMP tube) was still lower than that of w/o SMP group (silicone tube only) due to its anti-fibrotic function (Figure 4c) ($n = 3$ rabbits). d) Silicone material of the glaucoma device induces fibrotic tissue formation, which was suppressed by the release of anti-fibrotic drug (5-FU) from GelMA-$\beta$-CD in the SMP tube (small D) as seen in the H&E (left) and Masson's trichrome (right) stained sections with quantitative image analysis ($n = 4$). Data = mean $\pm$ standard deviation. *$p < 0.05$; ***$p < 0.001$ between lined groups from one-way ANOVA with Tukey's post hoc test. PCL, polycaprolactone.

**ADVANCED
SCIENCE NEWS**

www.advancedsciencenews.com
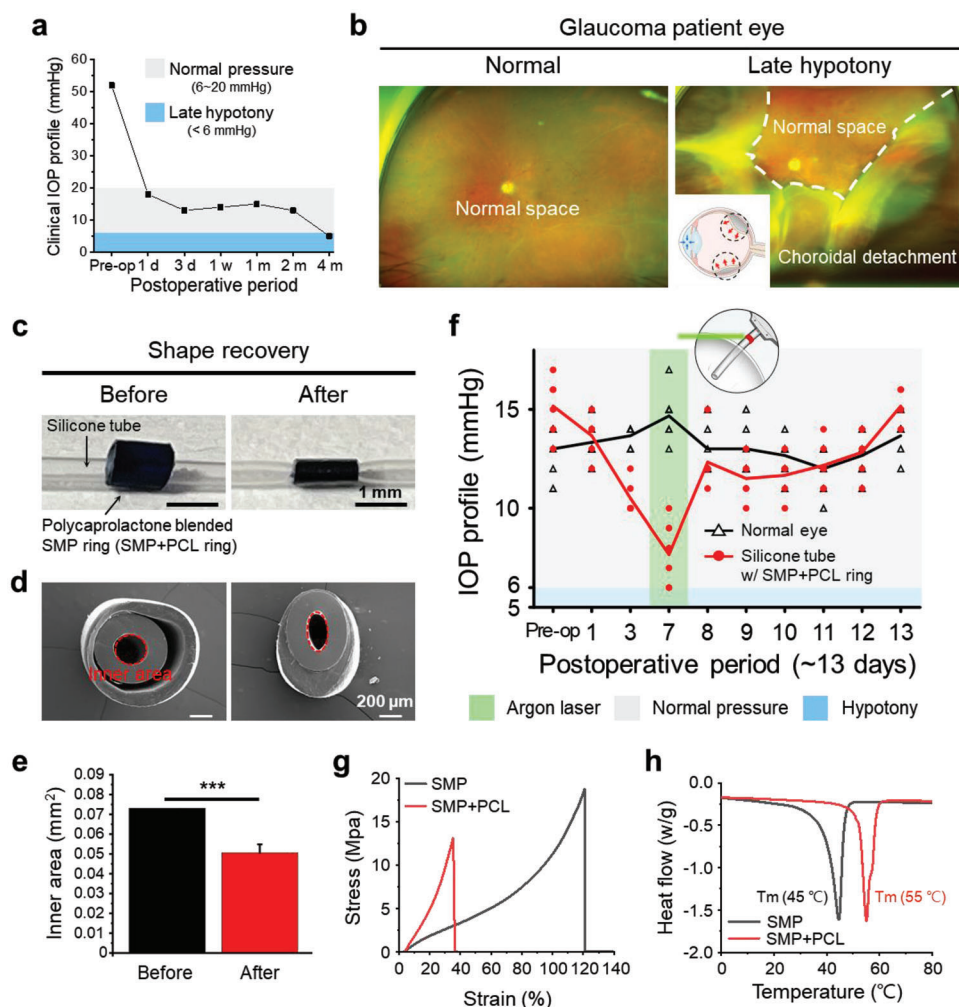
**ADVANCED
FUNCTIONAL
MATERIALS**

www.afm-journal.de

**Figure 5.** SMP+PCL ring as a safety lock to suppress late hypotony by externally squeezing a silicone tube. a) The clinical data indicate a sudden late IOP drop (>4 months) to the hypotony range in some cases after the implantation of the glaucoma device. b) In these late hypotony cases, some patients appeared to develop choroidal detachment and vision loss under prolonged severity, indicating the necessity of safeguards to remedy this condition. c) The SMP+PCL ring was developed to address this issue as argon laser shots induced shape recovery of the ring by squeezing the silicone tube, while it was externally wrapped around the tube. d) Consequently, the diameter of the silicone tube decreased significantly to reduce hypotony fluid drainage e) in SEM imaging, with quantitative Image analysis ($n = 3$). The ring was painted black to promote laser absorption. f) When the device was implanted in a normal rabbit eye, the IOP dropped continuously owing to the large diameter of the silicone tube until day 7. Immediately after the argon laser shots, the IOP drop stopped upon the squeezing shape recovery of the SMP+PCL ring with the decrease in the diameter of the silicone tube. Next, the IOP recovered to normal levels afterward until day 13 ($n = 6$ rabbits). g) SMP was blended with PCL because the modulus increased to promote the squeezing force in contrast to the relatively more elastic property of SMP only, as analyzed by a dynamic mechanical analyzer (DMA). h) The blending of SMP with PCL provided another user advantage because the increase in $T_m$ (melting temperature) by 10 °C could prevent unexpected squeezing by the ring when the argon laser shots to the SMP tube were incorrectly focused or transferred the heat to the ring, as analyzed by differential scanning calorimetry (DSC). Data = mean ± standard deviation. ***$p < 0.001$ between lined groups from one-way ANOVA with Tukey's post hoc test.

suggesting its safety, durability, and functionality. iii) When bacterial adhesion was tested on SMP silicone films for two days postseeding of *Pseudomonas aeruginosa*, the superior anti-biofilm effect of SMP was demonstrated by fewer crystal violet signals with fewer bacteria (Figure S8a, Supporting Information). Moreover, SMP exhibited the anti-fouling effect compared to silicone after 4 h-incubation in bovine serum albumin (BSA) solution with Bradford assay (Figure S8b, Supporting Information), indicating promising potential to suppress biofilm formation under long-term implantation.

## 2.5. Safety Lock Ring to Suppress Late Hypotony

The clinical data indicated a sudden late IOP drop (>4 months) in the hypotony range in some cases, after implantation of the glaucoma device (**Figure 5**a). In the late hypotony cases, some patients appeared to suffer choroidal detachment and vision loss under prolonged severity, clearly underscoring the need for safely alleviating this condition (Figure 5b). The SMP+PCL ring was designed to squeeze the silicone tube as an external wrap upon laser shots (Figure 5c; Video S4, Supporting Information), thereby

ADVANCED
SCIENCE NEWS

www.advancedsciencenews.com

ADVANCED
FUNCTIONAL
MATERIALS

www.afm-journal.de

significantly decreasing the silicone tube diameter and reducing fluid drainage, and consequently, hypotony (Figure 5d,e). The ring was painted black to promote laser absorption. When the device was implanted in a normal rabbit eye, the IOP dropped continuously owing to the large diameter of the silicone tube until day 7 (Figure 5f). Immediately after the argon laser treatment, the IOP drop stopped upon the squeezing shape recovery of the SMP+PCL ring (Video S4, Supporting Information). This was followed by the recovery of IOP to the normal range until day 13. Aside from modifying the PCL to GMA ratio in the SMP synthesis, blending the SMP with PCL (SMP+PCL) further increased both the modulus and $T_m$, compared to the relatively elastic and lower $T_m$ of SMP alone (Figure 5g). In this way, the squeezing force of safety lock ring was increased with the avoidance of co-operation with the SMP tube under the same laser $E$. In this way, the squeezing force of the safety lock ring was improved upon shape recovery by the higher $E$ transfer to avoid the simultaneous tube action which was set to occur with the lower $E$ input. The blending of SMP with PCL provided another advantage to users because the increase in $T_m$ by 10 °C could prevent unexpected squeezing by the ring, in the event when the argon laser shot to the SMP tube was incorrectly focused or when it transferred heat to the ring (Figure 5h).

## 3. Discussion

Unmet clinical needs have served as one of the most potent driving forces guiding continuous advances in implantable medical devices.[46–48] Present study is clearly aligned with this paradigm; our findings suggest the potential of a next generation of device design and function and posit the following salient points. First, the clinical argon laser system was used to induce shape recovery of the SMP tube because the pin-point delivery of laser E enabled site-specific control of the diameter increase with minimal influences on neighboring tissues. This control option is a powerful feature that aligns with the concepts of user-specified remote control, which has been applied to the current development of diagnostic and drug delivery systems. Second, the lumen coating to tube using biodegradable GelMA-$\beta$-CD/5-FU gel provided the dual benefits under implantation. i) The small inner diameter of the SMP tube gradually increased through the degradation of GelMA-$\beta$-CD/5-FU gel for two-week implantation, thereby preventing early hypotony. ii) The gel degradation also released 5-FU to prevent tissue fibrosis at the interface between sclera and tenon so that late ocular hypertension could be rescued. Hence, the current approach represents a beneficial addition to improve the functions of silicone drainage devices.[49–51] Third, the SMP+PCL ring was attached to the silicone device as a safety lock to reverse the one-way function of the SMP tube upon laser shots.

The implantation of glaucoma device sometimes results in outflow obstruction with fibrotic tissue formation, pigments, detritus of vitreous, lens cortex, and capsule, which has been usually observed upon implantation of small diameter tube device with collagen[52–54] or upon implantation into the deeper ocular areas (e.g., sulcus and pars plana). The SMP device was designed to place near the surface area (e.g., anterior chamber) to improve the laser responsiveness, so the issues have not been observed in the in vivo studies. In addition, 5-FU release significantly inhibited fibrotic tissue formation (Figure 4d). Even the implantation

of SMP tube into the deeper areas is not expected to raise the issues because the inner diameter of SMP devices gradually increases up to 250 μm which is substantially larger than that of a small tube device with collagen. In this respect, we believe that our device has promising potential as a new treatment modality for glaucoma patients with minimal side effects. Further clinical trials are needed to establish its efficacy and safety in real-world settings, and regulatory approval must be obtained prior to its widespread use.

As cases of late hypotony are not prevalent in clinical practice,[55,56] only one case has been tracked to demonstrate the result without error bars (Figure 5a). However, the silicone device-induced late hypotony results in the delayed restoration of vision, with blindness in severe cases,[29] justifying the use of a safety lock ring for the present approach. Furthermore, the animal model has not been established thus far, again because late hypotony is a rare occurrence. In the present study, the glaucoma model did not exhibit any pattern of late hypotony for 21–42 days after implantation of the silicone tube device (Figure 4b,c).

The entire study was designed to validate the two SMP functions of glaucoma drainage device so the rabbit model was approached to meet the duration of events in alignment with the two functions. First, the hypotony phase is usually seen for the first week as shown by the clinical data (Figure 1b), so the maintenance of small diameter by the drug-loaded gel function was examined for 14 days. During this period, the gel underwent gradual degradation with drug release, thereby increasing the drainage amount to be ready for the ocular hypertension phase with the prevention of tissue fibrosis. Second, the ocular hypertension phase lasts up to one month as seen in patients with glaucoma. Therefore, the rabbit model of glaucoma was maintained for 42 days, which is a little bit longer than the clinical indication. Although a previous study showed a longer period of rabbit model in which the cornea was replaced with perfluoropolyether,[57] the glaucoma model represents more severe damages, resulting in high mortality. Nonetheless, a longer period of examination in the rabbit model would help the validation of the stepwise increase in the tube diameter with the safety locking ring, which will be approached at the step of the preclinical study.

Other noteworthy findings of this study are summarized as follows. i) The design and function of the SMP devices were justified by tracking the clinical IOP profile of 127 glaucoma patients for one year. Therefore, this study suggests an advanced solution to address unmet clinical needs. ii) The three diameters were simulated by computational modeling of the flow and pressure. Hence, the detailed structural parameters before and after shape recovery were determined more precisely than the previous empirical and textbook-based methods, thereby presenting a meaningful prototype that can be applied for the development of other implantable medical devices. iii) The laser parameters were tuned in two steps to maximize the efficiency of the pin-point control within a clinic-friendly range. The use of a clinical laser system is significant because this first trial can influence the application of existing diagnostic and treatment machines for remotely operating implantable devices. iv) The hydrogel was designed to promote the drug loading capacity and enable sustained release.[58] In fact, several attempts were made to extract the aqueous humor of glaucomatous rabbits

to test the GelMA-$\beta$-CD degradation. However, the amount of eye fluid was merely a range of a few microliters which was too small for reliable analysis. Also, multiple trials to retrieve more fluid increased the mortality of test rabbits in conjunction with the severity of the glaucoma rabbit model. Hence, the in vivo degradation of the GelMA-$\beta$-CD hydrogel was additionally confirmed during 14 day-implantation into rabbit eyes by analyzing the cross-section of SMP tube in the SEM images (Figure S4c, Supporting Information). The PK parameters enabled the four stage analyses of drug release upon gel degradation according to a previous study.[59] During the first stage of drug release (0–1 day), the absence of $\beta$-CD in GelMA led to a fast increase in the released concentration of 5-FU within 1 day, as evidenced by the higher $C_{max}$ (0.59 ± 0.04 mg mL$^{-1}$) compared to the later time points (Figure S5, Supporting Information). The results indicate that the GelMA rapidly released the drug, resulting in the early burst effect. This burst effect appeared to be driven by inefficient encapsulation of 5-FU due to the absence of $\beta$-CD in GelMA. In contrast, the sustained 5-FU release from the GelMA-$\beta$-CD indicates that the conjugation of $\beta$-CD to GelMA improved the drug loading capacity with efficient encapsulation (Figure 2g).

During the second stage of drug release (1-3 day), GelMA showed a rapid decrease in the released concentration of 5-FU down to 50% of $C_{max}$. Interestingly, despite the absence of $\beta$-CD, 5-FU was not completely released from GelMA, indicating the control of 5-FU release by gelatin entanglement. The gelatin chains form an entangled network upon gelation, which restricts drug diffusion to release out of the gel. However, the GelMA-$\beta$-CD enabled a gradual release of 5-FU over the same period of time.

During the third stage of drug release (3–7 day), the released drug concentration from GelMA-$\beta$-CD/5-FU increased continuously to a maximum peak ($C_{max}$: 0.32 ± 0.02 mg mL$^{-1}$) by day 7. In contrast, the released drug concentration from GelMA kept being rapidly decreased, indicating the different mechanisms of release kinetics between the two gels. One possible driving factor is the gradual degradation of GelMA-$\beta$-CD compared to the burst degradation of GelMA (Figure 2h,i) as the gel degradation lets go drugs to release out from the entangled status with gelatin chains. As another driving factor, the inefficient encapsulation of drug by GelMA facilitates the rapid diffusion of drugs upon hydration. However, as drugs can be tightly held by GelMA-$\beta$-CD, drugs can be released only through the gel degradation, thereby enabling the sustained release. The results provide insight into a control mechanism of release kinetics depending on the target period of drug effect.

During the fourth stage of drug release (7–14 day), GelMA-$\beta$-CD kept a decremental pattern of released drug concentration, and GelMA released off most drugs. The PK analysis defined the sustained and burst releases of 5-FU by GelMA-$\beta$-CD/5-FU and GelMA, respectively. The sustained release was determined by the higher AUC and longer MRT, suggesting the efficient utility of GelMA-$\beta$-CD to prolong the anti-fibrotic effect of 5-FU under deployment of drainage device.

The amount of 5-FU was determined according to the clinically used fibrosis inhibitory dosage as previously reported.[31,60] This fine-tuned the dual benefits of diameter increase and anti-fibrotic drug release to fulfill the scope of the clinical requirement more efficiently.[61,62] v) The anti-biofilm effect of SMP surface with re-

duction of protein adsorption was validated, which can be applied to other implantable devices, such as bile duct stents,[63,64] nasolacrimal duct stents,[43] and dental devices.[65] vi) The concept of SMP functions was validated using a customized in vitro pressure system and a new rabbit model for glaucoma. In particular, the rabbit model exhibited the clinical pattern of IOP fluctuation when a drainage tube was implanted and clearly demonstrated the advantages of the SMP tube.

Despite the absence of the SMP tube, more than half of the patients with glaucoma did not show early hypotony until 2 weeks after implantation of the silicone device (Figure 1b) because the pre-op IOP range of those patients was high (≥28 mmHg), which rapidly decreased to the normal range. The declining trend of IOP in this population was similar to that of the other population, as the IOP range started below 28 mmHg and decreased to the hypotonic range upon implantation of the silicone device. This result indicates the possibility of the induction of ocular hypertension by inserting the SMP tube during this period, by reducing the tube diameter. However, among the 127 patients, 41 patients exhibited a hypotonic range during the early 2 weeks postimplantation of silicone device. As a single effector, the 14-day release of 5-FU might not be sufficient to suppress the tissue fibrosis if the device was implanted for a longer period of time up to 1 year. Therefore, GelMA-$\beta$-CD concentration-dependent changes in the degradation speed were demonstrated as an optional factor to prolong the drug release (Figure 2h). Furthermore, the stepwise increases in tube diameter can be suggested as an additional effector to reduce tissue fibrosis (Figure 4, and 5).

Herein, the effect of laser-induced diameter expansion on IOP reduction was validated by comparing the SMP tube insertion groups with and without argon laser irradiation. The anti-fibrotic effect of drug release on IOP control was confirmed by comparing the SMP tube insertion group without argon laser irradiation and the group without SMP tube insertion. First, the effect of reduced diameter on suppression of hypotony was demonstrated within 14 days upon insertion of SMP tube into a silicone tube in the rabbit glaucoma model (Figure 4b,c). This effect was not associated with exposure to argon laser, because laser operation was not performed during the initial 14 days. In further support of our finding, the drug-free effect of tube diameter reduction on suppression of IOP decline has been demonstrated previously.[34] Furthermore, when the SMP tube +/− laser groups were compared postdrug release in the same setting during the initial 14 days, the small tube diameter (-Laser) was not able to suppress the shift to ocular hypertension as much as the +Laser group with the expanded tube diameter after 14 days. The result indicates the clear advantage of diameter expansion in suppressing the late ocular hypertension under the same condition of drug release.

Second, the drug effect was discerned by comparing the w/o SMP tube group with the two w/SMP tube groups (+/− Laser) after 14 days (Figure 4c). Regardless of the laser-induced diameter expansion in the two w/SMP groups, the anti-fibrosis effect of 5-FU release maintained the normal IOP range in contrast with the incremental increase in ocular pressure to a hypertensive range as seen in the w/o SMP tube group. The three test groups started from the normal IOP range on day 14 with laser exposure, but only the w/o SMP group exhibited the incremental ocular

pressure continuously until the end of the experiment. In particular, the +laser group moved to the incremental IOP stage from days 15 to 16 (i.e., 1–2 days after laser exposure), indicating that the effect of tube diameter expansion started to attenuate. However, the w/o SMP group maintained a similar level of IOP during these two days, indicating that the anti-fibrosis drug mainly affected the suppression of IOP after day 16. The silicone tube only (w/o SMP tube) appeared to continue the momentum of tissue fibrosis to the later stage, whereas the release of an anti-fibrotic drug (w/SMP tube) during the early period served as an initial barrier to suppress the gradual development of tissue fibrosis. In addition, because of the biodegradable and biocompatible properties, the dominant PCL portion of SMP can serve as a depot to deliver various drugs under implantation as reported previously by others.[41,66,67] However, as the current SMP material exhibited only 1.5% degradation for 1 year (Figure S2d, Supporting Information) upon the accelerated aging test, a modification of SMP is required to deliver drugs (e.g., anti-inflammation) through proper degradation under implantation.

In future studies, mortality of rabbits with glaucoma should be taken into account to improve the reliability of the statistical analysis of the experiments, because herein, compared to normal rabbits ($n = 6$, Figure 5f), the number of glaucoma rabbits decreased to 5 (Figure 4b) and 3 (Figure 4c) owing to sudden deaths. An in-depth pharmacokinetic analysis should be performed to understand the drug release mechanism further; in the multiple trials conducted for this purpose in the present study, we observed increased mortality in rabbits with glaucoma owing to the collection of intraocular fluid. The drug release with the diameter increases of SMP tube prevented tissue fibrosis. As the SMP tube was inserted into a silicone tube, protein adsorption on the SMP surface was not expected to affect significantly the anti-fibrotic function. Indeed, the 42-day maintenance of the rabbit model did not exhibit the fibrotic response, indicating that the protein adsorption did not hamper the device performance. However, the long-term implantation will be approached at the stage of preclinical study to reveal whether the surface property (e.g., biofouling) of SMP plays a negative role in handling fibrosis formation.

The surface E and crystalline phase pattern of the SMP surface were identified as potential players, because variations in these factors can affect protein adsorption with microbial and mammalian cell attachment.[68,69] The anti-biofilm mechanism is still under study as the protein adsorption remains unchanged like PCL due to the absence of further surface modification. The dynamic behavior of the crystalline phase (e.g., tight alignment and structural fluctuation) in response to the temperature change might suppress the nucleation and growth of bacteria, thereby suppressing the biofilm formation. This mechanistic insight will be clearly provided after confirming the mechanism through further study. Current analytical systems have limitations in interpreting the dynamic changes in the surface parameters at the nanoscale level, upon controlling the external energy absorption. The interpretation becomes more difficult when biological players are introduced because of the heterogeneous behaviors of material and biological parameters depending on temperature, type, and duration. Moreover, because the SMP was painted black to help pin-point laser absorption, the appearance of eyes should be considered further.

## 4. Conclusions

The current study represents the significant therapeutic efficacy of a laser-responsive SMP device in treating glaucoma, which minimized side effects (e.g., hypotony and ocular hypertension) and undesired influences. Our device presented stepwise control of glaucoma drainage system for the first time. Until now, clinician-specified control of the IOP through the manipulation of a glaucoma drainage device has not been possible. The SMP tube was inserted into a silicone drainage tube, while the SMP ring was wrapped around the silicone tube externally. The insertion of SMP tube prevented early hypotony and late ocular hypertension. Early hypotony was prevented through the small inner diameter of the SMP tube, whereas late ocular hypertension was inhibited through the anti-fibrosis effect by gel degradation-mediated drug release and argon laser-triggered diameter expansion. Furthermore, silicone tube wrapped by SMP ring was squeezed by argon laser shots to prevent late hypotony. Resultantly, through the appropriate design of the new SMP device, the in vivo results suggest that both hypotony and ocular hypertension change can be prevented at the clinician's discretion. This is a factor that has the potential to greatly affect the success rate of glaucoma operation and play a major role in preventing blindness. In conclusion, our results suggest that the laser-responsive SMP presents a promising material in the field of implantable glaucoma medical devices that could guide the next generation of treatments, which are tailored to clinical needs.

## 5. Experimental Section

*Shape Memory Polymer (SMP) Synthesis*: All chemicals were purchased from Sigma-Aldrich (St. Louis, MO, USA). SMP was synthesized by ring-opening polymerization of ε-caprolactone (CL) and glycidyl methacrylate (GMA) monomers using an established protocol.[43] Briefly, CL (94 mmol), 1,6-hexanediol initiator (0.5 mmol), and hydroquinone (0.6 mmol, 1:10 molar ratio of hydroquinone to GMA) as auto-crosslinking inhibitor were made to react in a three-necked round bottom flask, under stirring at 110 °C for 10 min, followed by the reaction of GMA (6 mmol) with the mixture for 10 min. Subsequently, 1,5,7-triazabicyclo[4.4.0]dec-5-ene (TBD, 0.5 mmol) was dissolved in acetonitrile solvent (2 mL) and was made to react at 110 °C for 6 h under a nitrogen atmosphere. The reaction mixture was dissolved in chloroform (30 mL) after cooling to room temperature (25 °C), and then, a white precipitate was formed in cold diethyl ether (800 mL, 4 °C). The final SMP product was obtained via vacuum drying (OV4-30, Jeio Tech, Daejeon, Republic of Korea) at room temperature. The SMP+PCL blend was prepared by adding PCL (10% w/v, $M_w \sim 80\,000$) powder into SMP solution, fully dissolved in N-Methyl-2-pyrrolidone (NMP) at 37 °C, to enhance the polymer crystallinity and hardness, thereby improving elastic modulus with elevation of melting temperature ($T_m$). In this way, the squeezing force of safety lock ring was improved by preventing the co-incident operation with the SMP tube due to the $T_m$ elevation.

*Gelatin Methacryloyl (GelMA) Synthesis*: Photopolymerizable GelMA was synthesized by reacting methacrylate groups with the amine groups of gelatin molecules.[70] Briefly, gelatin powder from porcine skin (5 g, gel strength 300, type A, Sigma-Aldrich, St. Louis, MO, USA) was completely dissolved in phosphate buffer saline (PBS; 1X, pH 7.4, Welgene, Gyeongsangbuk-do, Republic of Korea) at 40 °C to prepare 10% (w/v) gelatin solution. Next, methacrylic anhydride (MA; 0.25 mL, Sigma-Aldrich, St. Louis, MO, USA) was added dropwise to the gelatin solution (50 mL) at a rate of 0.5 mL min⁻¹ under vigorous stirring for reaction at 50 °C for 3 h in the dark. Finally, the reaction was stopped by adding

**ADVANCED
SCIENCE NEWS**

www.advancedsciencenews.com

**ADVANCED
FUNCTIONAL
MATERIALS**

www.afm-journal.de

five-fold warm (40 °C) PBS to the reaction mixture. The unreacted MA and salts were then dialyzed in warm distilled water (40 °C) using a dialysis tube (molecular weight cut-off (MWCO): 12–14 kDa, Spectrum Laboratories Inc., New Brunswick, NJ, USA) for 5 days in the dark. The dialyzed solution was lyophilized to obtain a white porous foam of GelMA and stored at −30 °C until use.

*β-Cyclodextrin (β-CD) Conjugated GelMA (GelMA-β-CD) Synthesis*: GelMA-β-CD was synthesized to enhance the drug loading capacity using modifications of a previous report.[71] First, the GelMA backbone was conjugated with β-CD by introducing a carboxymethyl (CM) group into β-CD through the following steps. A mixture of β-CD (10 g, Sigma-Aldrich, St. Louis, MO, USA) and sodium hydroxide (NaOH; 9.3 g, Sigma-Aldrich, St. Louis, MO, USA) was dissolved in distilled water (37 mL) and reacted with a 16.3% (v/v) monochloroacetic acid solution (27 mL, Sigma-Aldrich, St. Louis, MO, USA) to introduce carboxylic groups into β-CD at 50 °C for 5 h. Then, the product was cooled to room temperature (25 °C), and the pH was adjusted to 6–7 using hydrochloric acid (HCl; Duksan, Gyeonggi-do, Republic of Korea) solution, followed by pouring into methanol to obtain a white precipitate. Finally, carboxymethylated β-CD (CM-β-CD) was obtained by vacuum drying the solid precipitate.

Next, GelMA (1 g) was completely dissolved in PBS (10% w/v, 10 ml) at 40 °C, and CM-β-CD (2 g) was added to 2-(N-morpholino)ethanesulfonic acid (MES; 0.1 M, pH 6, Bio Solution Co., Ltd., Seoul, Republic of Korea) buffer solution (10 mL). The carboxyl groups of CM-β-CD were activated by N-(3-Dimethylaminopropyl)-N′-ethylcarbodiimide hydrochloride (EDC; 120 mmol L$^{-1}$, Sigma-Aldrich, St. Louis, MO, USA) and N-hydroxysuccinimide (NHS; 60 mmol L$^{-1}$, Sigma-Aldrich, St. Louis, MO, USA) for 30 min. The GelMA solution (10 mL) was added to the CM-β-CD solution (10 mL) by adjusting the pH to 8–9 using NaOH (Duksan, Gyeonggi-do, Republic of Korea) solution. The reaction was continued for 12 h under vigorous stirring at 40 °C. Finally, the unreacted CM-β-CD and other impurities were dialyzed in warm distilled water (40 °C) using a dialysis tube (MWCO: 12–14 kDa) for 5 d under dark conditions.

*Material Characterization*: Successful conjugation and synthesis were confirmed by proton nuclear magnetic resonance ($^1$H-NMR; Avance III 400-MHz, Bruker Biospin, Billerica, MA, USA) spectroscopy, Fourier transform infrared (FTIR; Vertex 70, Bruker Biospin, Billerica, MA, USA) spectroscopy, dynamic mechanical analysis (DMA; Discovery DMA850, TA Instruments, New Castle, DE, USA), and differential scanning calorimetry (DSC; Discovery DSC25, TA Instruments, New Castle, DE, USA). The structure and molar composition were determined by $^1$H-NMR spectroscopy using a single z-axis gradient inverse probe at a frequency of 400 MHz. SMP and other materials were dissolved in chloroform-d (CDCl$_3$; Sigma-Aldrich, St. Louis, MO, USA) and dimethyl sulfoxide-d$_6$ (DMSO-d$_6$; Sigma-Aldrich, St. Louis, MO, USA). The results were further confirmed by FTIR spectroscopy using the KBr pellet method. The mechanical properties were characterized by analyzing the stress-strain curve using DMA at a controlled strain rate of 5 mm min$^{-1}$. The samples were prepared in the form of rectangles (8 [length] × 5 [width] × 0.25 [thickness] mm thick). Heat-flow-related thermal transitions were examined using DSC. The samples were heated to 150 °C, and then cooled to −80 °C for two cycles at a heating rate of 5 °C min$^{-1}$ under a nitrogen atmosphere. The glass transition temperature ($T_g$), melting temperature ($T_m$), crystallization temperature ($T_c$), melting enthalpy ($\Delta H_m$), and crystallization enthalpy ($\Delta H_c$) were determined using the DSC thermograms.

The number-average molecular weight ($M_n$) and weight-average molecular weight ($M_w$) were determined by gel permeation chromatography (GPC, Agilent technologies 1200 series, Agilent Technologies Inc., CA) against polystyrene standards, using a PLgel 51 μm Mixed-D column (300 mm, Ø = 7.5 mm) in tetrahydrofuran at a flow rate of 1 ml min$^{-1}$. SMP degradation was examined using the accelerated aging test following the American Society of Testing and Materials (ASTM) international standard 1980; the Equations (1),(2), and (3) to calculate the duration of a real-world life-time (RT) equivalent usage are defined below.

$$AAT = Desired\ (RT)/AAF \tag{1}$$

$$AAF = Q_{10}^{[(T_{AA}-T_{RT})/10]} \tag{2}$$

$$Q_{10} = 2.0 \tag{3}$$

where, AAT is the accelerated aging time;
  Desired (RT) is the desired duration of RT equivalent usage;
  AAF is the accelerated aging factor (rate), i.e., ratio of desired (RT) to AAT;
  $Q_{10}$ is the temperature coefficient, i.e., how quickly a material changes when the temperature is increased by 10 °C;
  $T_{AA}$ is the accelerated aging temperature;
  and $T_{RT}$ is 37 °C.
  Based on the aforementioned calculation, the following values were obtained for 12 months (Equations (4) and (5)).

$$AAF = 2.0^{3.3} = 9.85 \tag{4}$$

$$AAT = 365/9.85 = 37.01 \tag{5}$$

Following the obtained values, the accelerated aging condition was set by incubating SMP samples in normal saline (pH 7.4) at 70 ± 2 °C for 37 days. Then, degradation-mediated changes in the thermal properties were determined by DSC analysis. Accordingly, the weight loss (%) was calculated using the following Equation (6):

$$\frac{m_0 - m_a}{m_0} \times 100\% \tag{6}$$

where, $m_0$ is the initial mass and $m_a$ is the mass after degradation.

*Anti-Fibrotic Drug Loading*: Anti-fibrotic 5-Fluorouracil (5-FU) was loaded into the GelMA-β-CD hydrogel via hydrophobic interactions of β-CD to include 5-FU in a complex form. A GelMA-β-CD solution (5% w/v, 10 mL) and 5-FU powder (10 mg, Sigma-Aldrich, St. Louis, MO, USA) were mixed for 30 min under vigorous stirring to form the complex, which is also known as a host-guest interaction. The cavity of β-CD (host) accommodated 5-FU (guest) via hydrophobic interactions (GelMA-β-CD/5-FU), as confirmed by $^1$H-NMR. The CH proton peak of 5-FU appeared at δ = 7.6 ppm. The capacity of GelMA-β-CD to load 5-FU was evaluated (n = 3) by centrifuging the complex solution at 12 000 rpm for 10 min. The amount of free 5-FU in the supernatant was determined using an ultraviolet-visible (UV-Vis) spectrophotometer (Lambda25, PerkinElmer, Waltham, MA, USA) (absorbance: 269 nm), thereby performing reverse calculations for the amount of GelMA-β-CD/5-FU complex. GelMA (n = 3) without β-CD conjugation was used as the control. The degree of drug loading capacity for 5-FU was calculated using Equation (7):

$$Drug\ loading\ capacity\ for\ 5-FU\ drug\ (\%) = 100\% \times \frac{(A-B)}{A} \tag{7}$$

where, A is the total amount of 5-FU that reacts with GelMA or GelMA-β-CD; and B is the excluded amount of 5-FU that forms the complex in the supernatant.

The GelMA-β-CD/5-FU complex solution was lyophilized and stored at −30 °C until use.

*Computational Fluid Dynamics (CFD) Modeling*: CFD modeling was conducted to theoretically calculate the pressure difference (ΔP) and velocity between the inlet and outlet of the silicone drainage tube, with or without SMP tube insertion. Because clinical implantation of a glaucoma drainage tube often causes early hypotony owing to its large diameter, the insertion of an SMP tube with a smaller diameter in the middle part of the drainage tube was expected to address this issue. The inner diameter of the SMP tube was adjusted according to the clinical Δ P (>6 mm Hg), while the silicone tube diameter was fixed. The clinical definition of hypotony is IOP <6 mmHg; thus, the initial inner diameter (50 μm) of the inserted SMP tube was determined to generate an IOP of >6 mmHg.

ADVANCED
SCIENCE NEWS

www.advancedsciencenews.com

ADVANCED
FUNCTIONAL
MATERIALS

www.afm-journal.de

All CFD calculations were performed using the fluid flow (Fluent) mode in ANSYS (ANSYS workbench 2021 R2, Canonsburg, PA, USA). Since the *Reynolds number (NRe)* of the intraocular fluid was estimated to be less than ≈2000 (turbulent flow: $NRe > 2000$), a laminar flow condition was used to calculate $\Delta P$ and velocity upon SMP tube insertion, where a constant flow rate ($Q = 2.5\ \mu L\ min^{-1}$) and open boundary condition were applied. The obtained results were compared with the *Hagen–Poiseuille law* ($\Delta P = \frac{Q \cdot 8 \cdot \mu \cdot L}{\pi \cdot r^4}$, where $Q$, $\mu$, $L$, and $r$ are the fluid rate, viscosity, length, and radius, respectively).

*Pharmacokinetic (PK) Analysis*: A noncompartmental examination of relationship between 5-FU drug concentrations and time was carried out with pharmacokinetic (PK) analysis using WinNonlin 8.3 software (Certara, USA).[72] The maximum drug concentration ($C_{max}$) and the time ($T_{max}$) to reach $C_{max}$ were determined by analyzing the amount of 5-FU that each hydrogel type releases with calculating the half-life ($T_{1/2\lambda z}$) using Equation (8) as follows.

$$T_{1/2\lambda z} = \frac{0.693}{\lambda z} \tag{8}$$

Where $\lambda z$ is the first order rate constant that is the curve slope of terminal phase in changes of the concentration (c) as a function of time (t).

The area under the concentration-time curve (AUC) and the area under the first moment of concentration-time curve (AUMC) were calculated using a linear trapezoidal method with the Equations (9) and (10) as follows.

$$AUC_{t_1-t_2} = (t_2 - t_1) \cdot \frac{C_2 + C_1}{2} \tag{9}$$

$$AUMC_{t_1-t_2} = (t_2 - t_1) \cdot \frac{t_2 \cdot C_2 + t_1 \cdot C_1}{2} \tag{10}$$

Where $t_2 - t_1$ is a given time interval.

Subsequently, the mean residence time (MRT) was calculated using the following Equation (11).

$$MRT = \frac{AUMC}{AUC} = \frac{\int_0^\infty t \cdot C(t)\, dt}{\int_0^\infty C(t)\, dt} \tag{11}$$

*SMP Device Production*: The length and diameter of the anti-fibrotic drug-loaded SMP tubes were determined by CFD modeling, and SMP tube was fabricated as follows. SMP (1 g) was fully dissolved in NMP (1 mL, Sigma-Aldrich, St. Louis, MO, USA) at 37 °C and mixed with a photoinitiator, 2-hydroxy-1-(4-(hydroxyethoxy)phenyl)-2-methyl-1-propanone (Irgacure 2959; 5 mg, Sigma-Aldrich, St. Louis, MO, USA). Next, a poly(vinyl alcohol) (PVA; Raise3D, Irvine, CA, USA) wire was produced using a three-dimensional (3D) printer (Raised3D Pro2, Raise3D, Irvine, CA, USA) and used as a sacrificial material to generate the inner diameter of the SMP. A glass capillary tube (Paul Marienfeld GmbH & Co., KG, Lauda-Königshofen, Germany) was used as the outer mold. The PVA wire (outer diameter: 260 µm) was inserted into the glass capillary tube (inner diameter: 560 µm), followed by the injection of the SMP solution between the two layers. The SMP solution in the glass capillary tube was polymerized by UV irradiation (365 nm, 265 Mj cm$^{-2}$) for 100 s using a UV crosslinker (CL-3000L UV Crosslinker, Analytik Jena, Jena, Germany), and then, PVA was dissolved in distilled water for 3 days at 25 °C. The SMP tube was separated from the glass capillary tube and air dried.

The SMP tube underwent shape-programming as follows. i) The original length of the SMP tube was doubled in hot water at 55 °C ($T > T_m$), and this double length was determined considering the Poisson's ratio ($\nu = 0.2$) of SMP tube. ii) The elongated SMP tube was immersed in cold water at 4 °C ($T < T_m$) to fix the temporary shape, and iii) the temporary shape of the SMP tube was cut to a length of 3 mm, as determined by CFD modeling. Next, an anti-fibrotic drug (5-FU)-loaded GelMA hydrogel (GelMA-$\beta$-CD/5-FU hydrogel) was coated onto the intimal layer of the SMP tube to facilitate its release into the intraocular fluid. GelMA-$\beta$-CD/5-FU

solution (5% w/v) containing 0.5% (w/v) Irgacure 2959 was prepared in PBS at 37 °C. Then, a tungsten wire (outer diameter = 50 µm, GoodFellow, Delson, QC, Canada) was inserted into the temporary shape of the SMP tube as the outer mold (inner diameter: 200 µm), followed by the injection of the hydrogel solution in between the SMP tube and tungsten wire. The whole set was exposed to UV light for crosslinking GelMA by polymerization under the previously described conditions, and the tungsten wire was removed to create the inner diameter of the SMP tube. The actual diameter of SMP tube was measured by analyzing the images of SEM (MERLIN, Zeiss Merlin, Oberkochen, BW, Germany) ($n = 3$). The SMP tube was painted black with a waterproof ink to promote laser absorption.

To produce the SMP+PCL ring, SMP was blended with PCL to improve its mechanical properties, as determined by DMA. An SMP+PCL tube was produced following the same process used to make the SMP tube using a glass capillary tube as an outer mold (inner diameter: 800 µm) with intraluminal insertion of a PVA wire (outer diameter: 360 µm). The diameter of the SMP+PCL tube was enlarged by inserting a taper-shaped polylactic acid (PLA; Raise 3D, Irvine, CA, USA) mold with an incremental outer diameter of 200–1000 µm into the SMP+PCL tube. The tube position was adjusted to the targeted outer diameter range of the tapered PLA mold in hot water at 55 °C so that the inner diameter of SMP+PC tube increased from 200 to 1000 µm. Subsequently, the shape was fixed in cold water (4 °C). The SMP+PCL tube was cut into 1 mm long SMP+PCL rings. The ring diameter was examined using SEM with image analysis. The ring was painted black with a waterproof ink to promote laser absorption.

*Pressure Measurement System*: The drainage pressure of the silicone tube, with or without SMP tube insertion, was measured as previously described ($n = 3$).[34] The measurement system was customized to be equipped with a pressure transmitter (PNS, Nuritech, Incheon, Republic of Korea), pressure indicator (PD1, Nuritech, Incheon, Republic of Korea), three-way stopcock, silicone tube (2 [inner diameter] × 4 [outer diameter] mm, Korea Ace Scientific Co., Seoul, Republic of Korea), syringe, 30-gauge needle (Korea vaccine Co., LTD., Gyeonggi-do, Republic of Korea), and syringe pump (Standard PHD ULTRA CP Syringe Pump, Harvard Apparatus, Holliston, MA, USA). A silicone tube with small D, medium D, large D, or without SMP tube insertion was connected to the needle, and distilled water was injected into the test tube at a constant flow rate (25 µL min$^{-1}$) using the syringe pump. The pressure changes (mmHg) were recorded using a digital pressure indicator.

*GelMA-$\beta$-CD Degradation*: A consistent rod shape (4 mm diameter and 1 mm height) of GelMA-$\beta$-CD hydrogel with different concentrations (5, 7, and 10% (w/v)) was produced by crosslinking in a cylindrical UV system ($n = 3$). In vitro degradation was examined in PBS containing type I collagenase (1 unit/Ml, Gibco, Waltham, MA, USA) at 37 °C on a rocking shaker (50 rpm, RK-1D, Daihan Scientific, Kangwon-do, Republic of Korea), followed by replacing PBS every 2 days. Nondegraded hydrogels were collected each time, washed twice with distilled water, and lyophilized to measure their weight. The weight (%) of the nondegraded hydrogels was calculated using Equation (12):

$$\text{Weight (W \%) of nondegradation}$$

$$= (W_{\text{each time point}}/W_{\text{starting point}}) \times 100 \tag{12}$$

The hydrogel with the most rapid degradation was used in the rest of the experiments. In vivo degradation of the GelMA-$\beta$-CD hydrogel upon insertion into an SMP tube was determined during 14 day-implantation into rabbit eyes by analyzing SEM images at each time point.

*Anti-Fibrotic Drug Release*: In vitro release of 5-FU from the hydrogel with the most rapid degradation was determined by analyzing each cumulative profile with and without $\beta$-CD conjugation on GelMA ($n = 3$). The test samples were incubated under the same conditions as described above for hydrogel degradation. The test solution containing 5-FU postrelease from each hydrogel was collected at each time point, followed by replenishing the same amount of PBS. The amount of 5-FU released was determined using a UV-Vis spectrophotometer at 265 nm and a calibration plot.

**ADVANCED
SCIENCE NEWS**

www.advancedsciencenews.com

**ADVANCED
FUNCTIONAL
MATERIALS**

www.afm-journal.de

*Bacterial Adhesion*: In vitro bacterial adhesion was determined to confirm the superior anti-biofilm effect of SMP over silicone as reported previously.[43] Briefly, *Pseudomonas* (*P.*) *aeruginosa* (ATCC 9027, Seoul, Republic of Korea) was cultured in a tryptic soy agar (Sigma-Aldrich, St. Louis, MO, USA) at 37 °C until their growth reached the mid-exponential phase, 0.55 optical density of as indicated by an optical density of 0.55 obtained using a microplate spectrophotometer (600 nm, Infinite M Nano, Tecan, Männedorf, Switzerland). Sample films (1.5 × 1.5 cm) were prepared and incubated with *P. aeruginosa* at 37 °C for 48 h, followed by washing with distilled water to remove nonadhering bacteria. The samples were then air-dried for 40 min and stained with crystal violet (0.1%, Sigma-Aldrich, St. Louis, MO, USA) for 15 min for imaging by inverted optical microscopy (Leica DMi8, Leica Microsystems, Wetzlar, Germany) and SEM. For quantitative analysis, crystal violet dye was extracted from the bacteria using 95% (w/v) ethanol (Sigma-Aldrich, St. Louis, MO, USA), and the absorbance was measured at 600 nm using a microplate spectrophotometer.

*Protein Adsorption*: In vitro protein adsorption was determined to validate the superior anti-fouling effect of SMP to silicone. The film-type samples (1.5 × 1.5 cm) of SMP and silicone were incubated in bovine serum albumin (BSA) solution (2 mg mL$^{-1}$) for 4 h at 37 °C using a shaking incubator (KSI-200, KBT, Gyeonggi-do, Korea). BSA was chosen due to the adhesive property with the characteristics of a protein mixture. After incubation, samples were washed with PBS for 3 times to collect nonadsorbed BSA in the PBS together with the incubated BSA solution, followed by Bradford assay to quantify the nonadsorbed protein. Then, the amount of adsorbed protein was calculated by subtracting the amount of nonadsorbed protein from the total BSA amount. The incremental concentrations of BSA (0, 0.25, 0.5, 1, 1.4, 2, and 3 mg mL$^{-1}$) were used to draw a standard curve for determination of protein amount. Bradford reagent (B6919, Sigma, MO, USA) was incubated with each test solution for 5 min at room temperature, followed by absorbance reading at 595 nm in a spectrophotometer (A51119600, Thermo Scientific, MA, USA). The amount of BSA (mg) was calculated by applying the OD value into the standard curve.

*Shape Memory Function*: Since argon laser irradiation (Topcon PASCAL Streamline 532 nm Green Laser, Topcon Medical Laser Systems, Santa Clara, CA, USA) was used to induce the shape recovery of SMP tube, the energy density per unit surface area of tube was determined using Equation (13):

$$\text{Energy density } (\text{mJ cm}^{-2}) = A/B \qquad (13)$$

where, *A* is the laser energy (power [mW] × exposure time [ms]); and *B* is the surface area (cm$^2$).

Owing to the fixed laser irradiation (surface) area, the energy density was adjusted by varying the laser power (0–70 mJ). The shape recovery efficiency of the SMP tube was determined by changing a bent tube to a linear tube shape as sufficient laser energy per single shot was delivered. Next, the energy density was further examined to induce complete shape recovery in the range of 40–70 mJ by calculating the shape recovery ratio per single laser shot (%) (*n* = 3) using Equation (14):

$$\text{Shape recovery ratio per single laser shot } (\%) = (B/A) \times 100\% \qquad (14)$$

where, *A* is the length of the original shape of the SMP tube; and B is the length of the recovered shape of the SMP tube after a single laser shot.

The shape-recovery efficiency of the SMP+PCL ring was determined by analyzing the squeezed lumen area of the silicone tube using SEM images before and after argon laser irradiation (*n* = 3). The superior effect of the argon laser over water heat on shape recovery was examined by implanting tube samples into rabbit eyes. Two water samples at 25 °C and 50 °C were compared because the temperatures were below and above $T_m$, respectively, and proteins begin to denature above 50 °C. After the SMP tubes were inserted into silicone tubes, one was implanted into the intraocular position of the anterior chamber, while the other was positioned in an extraocular position on the cornea (control). The change in the length of the SMP tube at each position was analyzed upon water treatment. The energy density ($E_{Laser}$) of the argon laser was compared to the heat energy ($Q_{Water}$) of water

to determine its superior efficiency (%). The surface temperature of the rabbit cornea was measured using a thermal imaging camera (HT-18; Hti, Guangdong, China). The SMP tube and ring were painted black to promote laser absorption.

*Clinical Data Analysis*: The long-term intraocular pressure (IOP) profiles were obtained after implantation of silicone drainage devices (Model FP-7, New World Medical, Inc., Rancho Cucamonga, CA, USA) in patients with glaucoma (*n* = 127, between January 2015 and December 2016) at the Severance Hospital of the Yonsei University College of Medicine. This study was approved by the Institutional Review Board (IRB) of Severance Hospital (Seoul, Korea; IRB No. 3-2022-0432) and was conducted in accordance with the tenets of the Declaration of Helsinki. Clinical IOP data were collected before and during the 12-month implantation. The early hypotony and ocular hypertension phases were defined as IOP of <6 mmHg and >20 mmHg, respectively. The early hypotony phase was diagnosed by i) fundus examination of choroidal detachment using an Optos Daytona (Queensferry House, Carnegie Campus, Dunfermline, Scotland, United Kingdom) and ii) imaging of the anterior chamber using anterior segment optical coherence tomography (AS-OCT; TOMEY GmbH, Wiesbadener Strasse, Nuremberg, Germany). The late hypotony phase was diagnosed via examinations similar to those of the early hypotony phase. The ocular hypertension phase was diagnosed by considering the visual field index to analyze the rate of glaucoma progression using a Humphrey visual field analyzer (ZEISS Humphrey Field Analyzer 3, Carl Zeiss Meditec, Inc., Dublin, CA). The visual area of the eye was calculated as the percentage of the visible area (white) to the total area, including the blind part (black).

*Rabbit Study*: Rabbit experiments were approved by the Institutional Animal Care and Use Committee of the Yonsei Laboratory Animal Research Center (2021-0203) and conducted following the Use of Animals in Ophthalmic and Vision Research, as provided by the Association for Research in Vision and Ophthalmology Statement. New Zealand white rabbits (weight: 2.5–3 kg) were used to develop the glaucoma model by inserting dental composite resins (resin; BEAUTIFIL Flow, SHOFU DENTAL CORPORATION, San Marcos, CA, USA) into the anterior chamber to clog the drainage channel. This blocked the outflow of intraocular fluid and the IOP was elevated. Briefly, the rabbits were anesthetized by intramuscular injection of tiletamine-zolazepam (Zoletil 50; 10 mg kg$^{-1}$, Virbac Lab, Carros, France) and xylazine hydrochloride (Rompun; 2%, 5 mg kg$^{-1}$, Bayer Korea, Seoul, South Korea). Topical anesthesia was administered (proparacaine eye drops, Alcaine; Alcon, Fort Worth, Tex., USA) to control the pain. Paracentesis (0.05 mL) was performed using a 31-gauge needle (Korea Vaccine Co. Ltd., Gyeonggi-do, Republic of Korea). The resin (0.05 mL) was inserted into the anterior chamber, and 25% of the drainage channel was blocked by fixing the resin using a light-emitting diode (LED.H Curing light, Woodpecker, Wroclaw, Dolnoslaskie, Poland). The IOP was measured thrice per eye preoperatively and postoperatively on days 1, 3, and 7 to confirm the increase in IOP up to ≈60% as an indication of successful glaucoma modeling.

A silicone drainage tube with or without SMP tube insertion was implanted into the glaucomatous eyes of rabbits under the same anesthesia conditions as described above (*n* = 5). Corneal traction was first performed by placing a 7–0 Vicryl suture from the anterior chamber to the limbus, resulting in the downward rotation of the eye. Conjunctival resection was then performed in the supra-temporal region, followed by posterior dissection to separate Tenon's capsule from the sclera. A 23-gauge needle (Korea Vaccine Co., LTD., Gyeonggi-do, Republic of Korea) was inserted into the anterior chamber at a position 0.25 mm posterior to the limbus, followed by the insertion of sample tubes into the anterior chamber with the beveled side up through the needle tract. The sample tubes were anchored to the sclera using a 10–0 nylon suture, the conjunctiva was secured to the limbus using an interrupted 10-0 nylon suture, and ofloxacin ointment was applied to the eye. IOP was measured thrice under topical anesthesia at predetermined intervals for each eye using a tonometer (Tono-Pen AVIA, Reichert Technologies, Depew, USA). An argon laser was used to expand the inner diameter of the SMP tube and increase the drainage of intraocular fluid 14 days postimplantation. IOP measurements were continued for 42 days after implantation. The synergistic effect between the diameter expansion and release of

anti-fibrotic drugs by hydrogel degradation on IOP control was demonstrated in the late postoperative period. The three test groups were SMP tube insertion i) with and ii) without argon laser irradiation, and iii) no SMP tube insertion ($n = 3$). The effect of laser-induced diameter expansion on IOP reduction was validated by comparing the SMP tube insertion groups with and without argon laser irradiation. The anti-fibrotic effect of drug release on IOP control was confirmed by comparing the SMP tube insertion group without argon laser irradiation and the group without SMP tube insertion. The IOP profiles between days 14 and 21 were compared.

Because of the sudden IOP drop that often occurs for unknown reasons during the late postoperative period in patients with glaucoma after tube implantation, the SMP+PCL ring was developed to decrease the drainage amount of intraocular fluid, by shape recovery, to squeeze the silicone tube with an external wrap. Normal eyes were implanted with a silicone drainage tube (w/o SMP tube insertion) with the SMP+PCL ring, while normal eyes without any implantation served as a control ($n = 6$). The SMP+PCL ring was irradiated by an argon laser 7 days after implantation, followed by IOP measurement for the next 13 days.

*Histological Analysis:* Fibrotic tissue formation around the drainage tube was examined using tissues obtained after sacrificing the rabbits and then carefully excising the eyes to minimize disturbance of the bleb and implant. The tissues were fixed with 4% paraformaldehyde (CellNest, Gyeonggi-do, Republic of Korea) for 24 h, and the eyes were dissected with incisions passing through the middle of the bleb. After embedding the eye tissues in paraffin wax, the paraffin blocks were sectioned for hematoxylin and eosin (H&E) and Masson's trichrome staining. The fibrous tissue area was determined from four different photographs of Masson's trichrome staining, followed by quantitative image analyses using ImageJ (Fiji, National Institute of Health, MD, USA), and the fibrous tissue was indicated by blue color-positive collagen fibers.

*Statistical Analysis:* All experiments were performed with at least three replicates per condition. Statistical analyses were performed using one-way analysis of variance (ANOVA) with Tukey's post-hoc test to perform multiple pairwise comparisons between groups. All experimental data are presented as mean $\pm$ standard deviation, where $n$ denotes the number of samples obtained from independent experiments, or with dots and whisker plots, in which dots and whiskers are shown as average and minimum/maximum, respectively. Each experimental condition is mentioned in the corresponding figure legend. Differences were considered statistically significant at $p < 0.05$ (*$p < 0.05$, **$p < 0.01$, and ***$p < 0.001$). All statistical analyses were conducted with the following software programs: Excel, KyPlot 6.0 software (Kyenslab, Tokyo, Japan), Origin 2018 (OriginLab, Northampton, MA, USA), GraphPad Prism 5 (San Diego, CA, USA), and SigmaPlot V.12.0 (Systat Software Inc., San Jose, CA, USA).

## Supporting Information

Supporting Information is available from the Wiley Online Library or from the author.

## Conflict of Interest

The authors declare no conflict of interest.

## Data Availability Statement

The data that support the findings of this study are available from the corresponding author upon reasonable request.

[1] I. E. Araci, B. Su, S. R. Quake, Y. Mandel, *Nat. Med.* **2014**, *20*, 1074.

[2] Y. S. Choi, R. T. Yin, A. Pfenniger, J. Koo, R. Avila, K. B. Lee, S. W. Chen, G. Lee, G. Li, Y. Qiao, A. M. Berlioz, A. Kiss, S. Han, S. M. Lee, C. Li, Z. Xie, Y.-Y. Chen, A. Burrell, B. Geist, H. Jeong, J. Kim, H.-J. Yoon, A. Banks, S.-K. Kang, Z. J. Zhang, C. R. Haney, A. V. Sahakian, D. Johnson, T. Efimova, Y. Huang, G. D. Trachiotis, B. P. Knight, R. K. Arora, I. R. Efimov, J. A. Rogers, *Nat. Biotechnol.* **2021**, *39*, 1228.

[3] S. Sonmezoglu, J. R. Fineman, E. Maltepe, M. M. Maharbiz, *Nat. Biotechnol.* **2021**, *39*, 855.

[4] J. B. Jonas, T. Aung, R. R. Bourne, A. M. Bron, R. R. Ritch, S. P. Jonas, *Lancet* **2017**, *390*, 2183.

[5] W.-T. Liu, Y.-P. Cao, X.-H. Zhou, D. Han, *Adv. Sci.* **2022**, *9*, 2100617.

[6] P. Q. Nguyen, L. R. Soenksen, N. M. Donghia, N. M. A. Mari, H. D. Puig, A. Huang, R. Lee, S. Slomovic, T. Galbersanini, G. Lansberry, H. M. Sallum, E. M. Zhao, J. B. Niemi, J. J. Collins, *Nat. Biotechnol.* **2021**, *39*, 1366.

[7] C. Kathe, F. Michoud, P. Schönle, A. Rowald, N. Brun, J. Ravier, I. Furfaro, V. Paggi, K. Kim, S. Soloukey, L. Asboth, T. H. Hutson, I. Jelescu, A. Philippides, N. Alwahab, J. Gandar, D. Huber, C. I. D. Zeeuw, Q. Barraud, Q. Huang, S. P. Lacour, G. Courtine, *Nat. Biotechnol.* **2022**, *40*, 198.

[8] Y. Zhu, S. Li, J. Li, N. Falcone, Q. Cui, S. Shah, M. C. Hartel, N. Yu, P. Young, N. R. D. Barros, Z. Wu, R. Haghniaz, M. Ermis, C. Wang, H. Kang, J. Lee, S. Karamikamkar, S. Ahadian, V. Jucaud, M. R. Dokmeci, H.-J. Kim, A. Khademhosseini, *Adv. Mater.* **2022**, *34*, 2108389.

[9] D. D. Nguyen, L.-J. Luo, J.-Y. Lai, *Adv. Healthcare Mater.* **2019**, *8*, 1900702.

[10] L.-J. Luo, D. D. Nguyen, J.-Y. Lai, *J Control Release* **2020**, *317*, 246.

[11] L.-J. Luo, D. D. Nguyen, J.-Y. Lai, *Theranostics* **2021**, *11*, 5447.

[12] D. D. Nguyen, C.-H. Yao, S. J. Lue, C.-J. Yang, Y.-H. Su, C.-C. Huang, J.-Y. Lai, *Chem. Eng. J.* **2023**, *451*, 138620.

[13] R. Chen, F. Gore, Q.-A. Nguyen, C. Ramakrishnan, S. Patel, S. H. Kim, M. Raffiee, Y. S. Kim, B. Hsueh, E. K. Magnusson, I. Soltesz, K. Deisseroth, *Nat. Biotechnol.* **2021**, *39*, 161.

[14] D. Hua, A. Harizaj, M. Wels, T. Brans, S. Stremersch, H. D. Keersmaecker, E. B. Fernandez, F. Vanhaecke, D. Roels, K. Braeckmans, R. Xiong, C. Huang, S. C. D. Smedt, F. Sauvage, *Adv. Mater.* **2021**, *33*, 2008379.

[15] N. Wang, S. K. Chintala, M. E. Fini, J. S. Schuman, *Nat. Med.* **2001**, *7*, 304.

[16] R. N. Weinreb, C. K. S. Leung, J. G. Crowston, F. A. Medeiros, D. S. Friedman, J. L. Wiggs, K. R. Martin, *Nat Rev Dis Primers* **2016**, *2*, 16067.

[17] K. S. Lim, B. D. S. Allan, A. W. Lloyd, A. Muir, P. T. Khaw, *Br. J. Ophthalmol.* **1998**, *82*, 1083.

[18] K. S. Schwartz, R. K. Lee, S. J. Gedde, *Curr. Opin. Ophthalmol.* **2006**, *17*, 181.

**ADVANCED
SCIENCE NEWS**

www.advancedsciencenews.com

**ADVANCED
FUNCTIONAL
MATERIALS**

www.afm-journal.de

[19]  I. C. F. Pereira, R. V. D. Wijdeven, H. M. Wyss, H. J. M. Beckers, J. M. J. D. Toonder, *Eye* **2021**, *35*, 3202.

[20]  I. Suiier, D. S. Greenfield, M. P. Miller, M. T. Nicolela, P. F. Palmberg, *Ophthalmology* **1997**, *104*, 207.

[21]  P. G. Christakis, D. Zhang, D. L. Budenz, K. Barthon, J. C. Tsai, I. I. K. Ahmed, *Am. J. Ophthalmol.* **2017**, *176*, 118.

[22]  G. S. Megevand, A. M. Bron, *Prog. Retinal Eye Res.* **2021**, *81*, 100879.

[23]  R. S. Ayyala, D. Zurakowski, J. A. Smith, R. Monshizadeh, P. A. Netland, D. W. Richards, W. E. Layden, *Ophthalmology* **1998**, *105*, 1968.

[24]  K. N. Mahdavi, J. Caprioli, *Am. J. Ophthalmol.* **2003**, *136*, 1001.

[25]  J. T. Jacob, O. J. Lacour, C. F. Burgoyne, *Biomaterials* **2001**, *22*, 3329.

[26]  M. A. Wronska, I. B. O'Connor, M. A. Tilbury, A. Srivastava, J. G. Wall, *Adv. Mater.* **2016**, *28*, 5485.

[27]  J. C. Doloff, O. Veiseh, R. d. Mezerville, M. Sforza, T. A. Perry, J. Haupt, M. Jamiel, C. Chambers, A. Nash, S. A. Fotovat, J. L. Stelzel, S. J. Bauer, S. Y. Neshat, J. Hancock, N. A. Romero, Y. E. Hidalgo, I. M. Leiva, A. M. Munchoz, A. Bayat, B. M. Kinney, H. C. Hodges, R. N. Miranda, M. W. Clemens, R. Langer, *Nat. Biomed. Eng.* **2021**, *5*, 1115.

[28]  C. Horejs, *Nat. Rev. Mater.* **2021**, *6*, 554.

[29]  A. Rosentreter, S. Gaki, A. Lappas, C. Cursiefen, T. S. Dietlein, *Br. J. Ophthalmol.* **2013**, *97*, 715.

[30]  W. Ewa, P.-D. Joanna, H. Iwona, M.-H. Marta, *Int Ophthalmol* **2020**, *40*, 235.

[31]  E. Green, M. Wilkins, C. Bunce, R. Wormald, *Cochrane Database Syst Rev* **2014**, *3*, CD001132.

[32]  A. Z. M. Badruddoza, A. S. H. Tay, P. Y. Tan, K. Hidajat, M. S. Uddin, *J. Hazard. Mater.* **2011**, *185*, 1177.

[33]  H. Izawa, K. Yamamoto, S. Yoshihashi, S. Ifuku, M. Morimoto, H. Saimoto, *Polym J* **2016**, *48*, 203.

[34]  W. T. Oh, J. B. Lee, W. Choi, H. W. Bae, C. S. Kim, C. Y. Kim, H.-J. Sung, *ACS Biomater. Sci. Eng.* **2020**, *6*, 3784.

[35]  Y. Xia, Y. He, F. Zhang, Y. Liu, J. Leng, *Adv. Mater.* **2021**, *33*, 2000713.

[36]  J.-Y. Lai, L.-J. Luo, *Eur. J. Pharm Biopharm.* **2017**, *113*, 140.

[37]  J. Li, T. Feng, W. Yang, Y. Xu, S. Wang, H. Cai, Z. Liu, H. Qiang, J. Zhang, *Drug Delivery* **2021**, *28*, 1890.

[38]  V. Suvarna, B. Bore, C. Bhawar, R. Mallya, *Biomed. Pharmacother.* **2022**, *149*, 112862.

[39]  N. A. Rohner, S. J. Schomisch, J. M. Marks, H. A. V. Recum, *Mol. Pharmaceutics* **2019**, *16*, 1766.

[40]  D. Loessner, C. Meinert, E. Kaemmerer, L. C. Martine, K. Yue, P. A. Levett, T. J. Klein, F. P. W. Melchels, A. Khademhosseini, D. W. Hutmacher, *Nat. Protoc.* **2016**, *11*, 727.

[41]  D. D. Nguyen, L.-J. Luo, C.-J. Yang, J.-Y. Lai, *ACS Nano* **2023**, *17*, 168.

[42]  E. L. A. Briggs, T. Toh, R. Eri, A. W. Hewitt, A. L. Cook, *Mol. Vision* **2015**, *21*, 1162.

[43]  J. Y. Park, J. B. Lee, W. B. Shin, M.-L. Kang, Y. C. Shin, D. H. Son, S. W. Yi, J.-K. Yoon, J. Y. Kim, J. S. Ko, C.-S. Kim, J. S. Yoon, H.-J. Sung, *Acta Biomater.* **2020**, *101*, 273.

[44]  Y. C. Shin, J. B. Lee, D.-H. Kim, T. Kim, G. Alexander, Y. M. Shin, J. Y. Park, S. Baek, J.-K. Yoon, Y. J. Lee, G. M. Seon, M. H. Lee, M.-L. Kang, W. S. Jang, J.-C. Park, H.-W. Jun, Y. T. Kim, H.-J. Sung, *Adv. Mater.* **2019**, *31*, 1904476.

[45]  S. W. Yi, Y. M. Shin, J. B. Lee, J. Y. Park, D.-H. Kim, W. Baek, J.-K. Yoon, D. G. Kim, I. S. Shin, C.-S. Kim, M.-L. Kang, J. W. Yang, H.-J. Sung, *Small* **2021**, *18*, 2007297.

[46]  S. R. Patel, C. M. Lieber, *Nat. Biotechnol.* **2019**, *37*, 1007.

[47]  C. Li, C. Guo, V. Fitzpatrick, A. Ibrahim, M. J. Zwierstra, P. Hanna, A. Lechtig, A. Nazarian, S. J. Lin, D. L. Kaplan, *Nat. Rev. Mater.* **2020**, *5*, 61.

[48]  G.-H. Lee, H. Moon, H. Kim, G. H. Lee, W. Kwon, S. Yoo, D. Myung, S. H. Yun, Z. Bao, S. K. Hahn, *Nat. Rev. Mater.* **2020**, *5*, 149.

[49]  R. A. Hill, D. K. Heuer, G. Baerveldt, D. S. Minckler, J. F. Martone, *Ophthalmology* **1991**, *98*, 1042.

[50]  D. S. Minckler, D. K. Heuer, B. Hasty, G. Baerveldt, R. C. Cutting, W. E. Barlow, *Ophthalmology* **1988**, *9*, 1181.

[51]  S. W. Siegner, P. A. Netland, R. C. U. Jr, A. S. Williams, D. W. Richards, M. A. Latina, J. D. Brandt, *Symp. Ocul. Ther.* **1995**, *102*, 1298.

[52]  R. Razeghinejad, Ophthalmol, *Glaucoma.* **2020**, *3*, 376.

[53]  D. C. Sousa, I. Leal, L. A. Pinto, *Ophthalmol Glaucoma* **2018**, *1*, 81.

[54]  K. Mansouri, K. Gillmann, G. E. Bravetti, *J Curr Glaucoma Pract* **2019**, *13*, 113.

[55]  E. N. Burney, H. A. Quigley, A. L. Robin, *Am. J. Ophthalmol.* **1987**, *103*, 685.

[56]  B. A. Francis, M. Wang, H. Lei, L. T. Du, D. S. Minckler, R. L. Green, C. Roland, *Br. J. Ophthalmol.* **2005**, *89*, 17.

[57]  R. Z. Xie, M. D. M. Evans, B. Bojarski, T. C. Hughes, G. Y. Chan, X. Nguyen, J. S. Wilkie, K. M. McLean, A. Vannas, D. F. Sweeney, *Invest. Ophthalmol. Vis. Sci.* **2006**, *47*, 574.

[58]  D. D. Nguyen, J.-Y. Lai, *Polym. Chem.* **2020**, *11*, 6988.

[59]  S.-F. Chou, L.-J. Luo, J.-Y. Lai, *Acta Biomater.* **2016**, *38*, 116.

[60]  E. K. Reinthal, P. O. Denk, M. Grub, D. Besch, K. U. Bartz-Schmidt, *Graefes Arch Clin Exp Ophthalmol* **2006**, *3*, 369.

[61]  A. D. Tagalakis, S. Madaan, S. D. Larsen, R. R. Neubig, P. T. Khaw, I. Rodrigues, S. Goyal, K. S. Lim, C. Y.-W. Man, *J. Nanobiotechnol.* **2018**, *16*, 97.

[62]  A. Dong, L. Han, Z. Shao, P. Fan, X. Zhou, H. Yuan, *ACS Appl Mater Interfaces* **2019**, *11*, 10244.

[63]  A. B. Ballinger, J. A. Woolley, M. Ahmed, H. Mulcahy, E. M. Alstead, J. Landon, M. L. Clark, M. J. Farthing, *Gut* **1998**, *42*, 555.

[64]  A. Swidsinski, P. Schlien, A. Pernthaler, U. Gottschalk, E. Bärlehner, G. Decker, S. Swidsinski, J. Strassburg, V. Loening-Baucke, U. Hoffmann, D. Seehofer, L. P. Hale, H. Lochs, *Gut* **2005**, *54*, 388.

[65]  C. R. Arciola, D. Campoccia, L. Montanaro, *Nat. Rev. Microbiol.* **2018**, *16*, 397.

[66]  Y. Arun, R. Ghosh, A. J. Domb, *Adv. Funct. Mater.* **2021**, *31*, 2010284.

[67]  D. Y. Cho, H. Cho, K. Kwon, M. Yu, E. Lee, K. M. Huh, D. H. Lee, H. C. Kang, *Adv. Funct. Mater.* **2015**, *25*, 5479.

[68]  H. Chen, L. Yuan, W.-Q. Song, Z. Wu, D. Li, *Prog. Polym. Sci.* **2008**, *33*, 1059.

[69]  A. E. Nel, L. Mädler, D. Velegol, T. Xia, E. M. V. Hoek, P. Somasundaran, F. Klaessig, V. Castranova, M. Thompson, *Nat. Mater.* **2009**, *8*, 543.

[70]  K. Lee, Y. Chen, T. Yoshitomi, N. Kawazoe, Y. Yang, G. Chen, *Adv. Healthcare Mater.* **2020**, *9*, 2000617.

[71]  X. Zhou, Z. Luo, A. Baidya, H.-j. Kim, C. Wang, X. Jiang, M. Qu, J. Zhu, L. Ren, F. Vajhadin, P. Tebon, N. Zhang, Y. Xue, Y. Feng, C. Xue, Y. Chen, K. J. Lee, J. Lee, S. Zhang, C. Xu, N. Ashammakhi, S. Ahadian, M. R. Dokmeci, Z. Gu, W. Sun, A. Khademhosseini, *Adv. Healthcare Mater.* **2020**, *9*, 2000527.

[72]  C. Zhang, G. Li, Y. Wang, F. Cui, J. Zhang, Q. Huang, *Int. J. Pharm.* **2012**, *436*, 272.